Hadronization in Nuclei by Deep Inelastic Electron Scattering

(A new proposal to Jefferson Lab 12 GeV PAC32)

G.D. Cates, D. Crabb, D. Day, R. Lindgren, N. Liyanage,
B.E. Norum (spokesperson), V. Nelyubin, O. Rondon-Aramayo,
K. Slifer, L.C. Smith, K. Wang (spokesperson), X. Zheng
University of Virginia, Charlottesville, Virginia

A. Afanasev, W. Brooks, A. Camsonne, J.P. Chen (spokesperson),
E. Chudakov, A. Deur,J. Gomez, O. Hansen, D.W. Higinbotham,
J. LaRose, S. Nanda, A. Saha, B. Wojtsekhowski
Jefferson Lab, Newport News, Virginia

Y. Jiang, H.J. Lu(spokesperson), X.H. Yan , Y.X. Ye
University of Science and Technology of China, Hefei, Anhui, China

L. Weinstein
Old Dominion University, Norfolk, Virginia

L. Tang, Z. Ye, L. Yuan
Hampton University, Hampton, Virginia

C.C. Chang
University of Maryland, College Park, Maryland

W. Bertozzi, S. Gilad, J. Huang, B. Moffit, P. Monaghan,
N. Muangma, A. Pucket, Y. Qing, X.-H. Zhan
MIT, Cambridge, Massachusetts

S. Choi, Ho. Kang, Hy. Kang, B. Lee, Y. Oh, J. Song
Seoul National University, Seoul 151-747, Korea

Z.-E. Meziani, B. Sawatzky
Temple University, Philadelphia, Pennsylvania

X. Jiang
Rutgers University, New Brunswick, NJ

E. Cisnani, F. Cusanno, S. Frullani, F. Garibaldi
INFN Roma 1 Gr. Coll., Sanitá, Rome, Italy

G.M. Urciuoli
INFN Roma 1, Rome, Italy

R.De Leo, L. Lagamba, S. Marrone
INFN Bari, Bari, Italy

M. Iodice
INFN Roma 3, Rome, Italy

X. Wang
Lawrence Berkeley National Laboratory, Berkeley, California

J. Feng, X. Li, S.H. Zhou
Institute of Atomic Energy, Beijing, China

S. Širca
University of Ljubljana, Ljubljana, Slovenia

K.A. Aniol
California State University , Los Angeles, California

W. Korsch
University of Kentucky, Lexington, Kentucky

B.T. Hu, W. Luo, H.Y. Yang, X.D. Zhang, Y. Zhang
Lanzhou University, Lanzhou, China

L. Li, P.Z. Ning, Y. Xu, C.X. Yu
Nankai University, Tianjin, China

B.Q. Ma
Beijing University, Beijing, China

Abstract

Semi-inclusive measurements of deep inelastic electron scattering from nuclei provide a unique testing ground to study the process of hadron formation. The effects of the nuclear medium can be extracted by comparing the production under different kinematic conditions of different hadronic species from different target nuclei. The 11 GeV beam to be available at JLAB will provide the required kinematic flexibility to extract a range of information.

In order to study the hadronization process one must isolate the high Q^2 data from the much more probable low Q^2 events. The Hall C HMS spectrometer and the projected SHMS with its first-generation detector package will be used for electron and meson detection. The high luminosity available in Hall C will make it possible to obtain reasonable counting rates in spite of the small cross sections. Moreover, the excellent particle identification will provide data separately on pion, kaon, and proton electroproduction.

The high precision CLAS data obtained with 5 GeV electrons have shown great promise for improving our understanding of the space-time evolution from quark propagation to hadronization at moderate values of Q^2. The proposed measurements will take our understanding to a new level.

The data obtained at RHIC have been interpreted in terms of a high density, high temperature quark-gluon liquid. The proposed measurements will contribute significantly to the interpretation of the RHIC results. Moreover, various theoretical approaches have been developed to understand the available experimental data on hadronization, but the data do not discriminate effectively among the models. The proposed Hall C experiment will provide precise data at higher Q^2, sufficient to discriminate among models. The demonstrated performance and on-going upgrade of the RICH detector will allow a clean kaon and pion separation. This will be crucial in distinguishing among different mechanisms in hadronization.

We will measure multiplicity ratios on LH_2, LD_2, carbon, copper, and tungsten targets over the range Q^2 = 2.5 - 6 $(GeV/c)^2$. In so doing we will map out the Q^2, P_T, A and z dependences.

1 Introduction

Deep Inelastic (lepton) Scattering (DIS) has played an important role in our study of the structure of the nucleon. Due to the weakness of the electromagnetic interaction, the virtual photon can deliver a large amount of momentum to a single quark inside the nucleon without disturbing the environment strongly. As a result, a struck quark can recoil with high momentum. According to QCD, quarks are confined by the color field. Therefore, a struck quark must go through a hadronization process and ultimately materialize in a form of a hadron or hadron jet. A fuller understanding of this process requires a semi-inclusive measurement where the leading hadron is detected in coincidence with the scattered electron.

A finite nuclear target offers a unique environment in which to study the space-time evolution of the struck quark which will interact with other partons before it is hadronized. In the case of a nucleon target, the quark will be more likely to hadronize outside due to the small nucleon size. However, in the case of a large nuclear target, the struck quark or leading hadron (the one carrying the largest fraction of the momentum) must pass through and interact with the rest of the nuclear constituents. Consequently, the process is sensitive to the mechanism of quark propagation inside the nuclear medium, which is of primary interest to the theory of QCD.

The evolution from the leading quark to a hadron can be characterized by a formation length, Λ_h, a measure of the average distance traveled during the hadronization process. To first approximation, Λ_h can be expected to scale with ν, the energy transfered by the virtual photon:

$$\Lambda_h \approx \nu \times 1 \ fm/GeV.$$

Thus, if ν is large, say 50 GeV, the quark will most likely materialize at a distance well outside of even a heavy nucleus. In this case, the observed A-dependent effects can be attributed to the interaction between the leading quark and the remnant of the nucleus. These effects were shown to be small by the EMC[1] and TMC[2] data. However, as ν is decreased, the hadrons possibly will be formed inside the target nucleus and then interact with the nuclear constituents before leaving the nucleus. As a result, the hadron spectrum will be diluted.

Our understanding of the space-time development of a hadronic shower, although of fundamental importance, has not progressed much beyond an elementary level. The experimental investigations so far have been limited by the available beams and detectors. The theoretical descriptions of quark-nucleon cross sections and hadronic formation lengths are still more qualitative than quantitative. It is essential to perform carefully controlled measurements of deep inelastic electroproduction of hadrons from a variety of nuclear targets with high precision. Knowledge of the momentum and multiplicity distributions of the reaction products for a variety of nuclear targets and over a wide kinematic range will be required before we can have a sound knowledge of nuclear medium effects on the struck quark and the leading hadron. As was pointed out by Bjorken [3], the space-time evolution of the final states in the parton model is important in that *it bears upon very basic questions of the dynamics of deep inelastic process. Looking in detail at the space-time evolution of the process, say in electroproduction, from the time when the quark is hit to the time when the final hadrons emerge as asymptotic states one should learn something about the dynamics of confinement.* For this purpose, the *A-dependence of the spectrum of energetic hadrons produced in electroproduction could turn out to be quite interesting.*

The measurement at $\nu = 6$ GeV will provide important input to the interpretation and understanding of RHIC results. The RHIC data have suggested that a quark-gluon liquid (QGL) state is created in collisions of two relativistic gold ions. The fact that it behaves more like a liquid than a gas gives us insight into the earliest moments of the universe. A great deal of theoretical and experimental activity is aimed at understanding the properties of this new form of hot matter. The process by which this QGL interacts with the vacuum and produces hadrons is called hadronization. The complexity of the process of hadronization increases with energy. To obtain a solid understanding it is essential to first examine hadronization at relatively low energies, i.e., in "cold matter." It has been suggested that other reactions, such as the deuteron-gold collisions, be used for this purpose. However, such reactions are complicated by the multi-quark composition of both particles. By comparison, deep inelastic electron scattering provides a relatively clean and simple means of focusing in on quark propagation and hadronization processes. Consequently, the data from this experiment will constitute a decisive step towards an understanding of the experimental results on quark

behavior in hot matter.

In addition to the existing data from HERMES, high precision data at 5 GeV over a continuous and broad kinematic range have been acquired by the CLAS Collaboration. However, since the detectors in both of these experiments have large acceptances, the data are dominated by events in which the electron scatters through a small scattering angle or, equivalently, at low Q^2. High precision data at high Q^2's are at least equally important.

In order to study this process at high Q^2 one must selectively isolate such events in order to avoid being overwhelmed by the much more probable low Q^2 events. The restrictive acceptances of the Hall C HMS and SHMS spectrometers are ideal for such a study. The high luminosity available in Hall C makes it possible to obtain reasonable counting rates in spite of the small cross sections. Moreover, the excellent particle identification will provide data separately on pion, kaon, and proton electroproduction. The ability to observe separately the process of hadronization into different hadronic species will be very important to obtaining an understanding of the physical processes involved. The SHMS provides an excellent separation of electron from hadron (e/h discrimination is 1000:1 at 98% efficiency) and π from kaon (π/K discrimination is 100:1 at 95% efficiency). Improvement at the higher momenta can be accomplished by adjusting the gap and changing the index of refraction of the radiator. The sensitivity to the flavor degree of freedom provided by the pion and kaon separation is an important feature of the experiment. The formation lengths for the two species are significantly different and, therefore, can be expected to exhibit different sensitivities to the size of the target nucleus. This selectivity will provide important constraints for theoretical descriptions of the process.

The hadronization process is sensitive to the mass of the target (A), a variety of kinematic quantities (Q^2, ν, P_T, and z), and a variety of mechanisms (quark propagation, pre-hadron state and hadron formation, the Cronin effect, gluon radiation, Landau-Pomeranchuck effect, etc). To distinguish one effect from another, data in a wide range of narrow kinematic bins will be required. The experimental data will shed light on the mechanism of fast quark propagation in nuclear matter and the formation length of hadrons following a hard collision. The P_T broadening of the observed hadron dis-

tributions could provide a convincing signature for the rescattering of the quark inside the nuclear medium.

We propose to study nuclear effects in the process of hadronization via the reaction $A\,(e, e'[\pi, K, p])\,X$ using a 11 GeV beam and several kinematic settings. Four targets will be used: deuterium, carbon, copper and tungsten. The HRSR will be used to detect electrons and HRSL will be used to detect hadrons (pions, kaons, and protons). The z-dependence of the ratios of the fragmentation functions for $A > 2$ to that for deuterium will be a measure of the formation time of the hadronization; the z, P_T and A dependencies will show possible signatures of the LPM effect; the dependence on the hadron mass will help to reveal whether the hadron is formed inside the target nucleus; the data from different P_T coverages will enable us to evaluate the multiple scattering of fast quarks inside nuclei. Information from the proposed experiment will also serve as an important input to the interpretation of the RHIC data. Due to the complexity of the physics involved, and due to the dependence on multiple kinematic variables, data with high precision in small bins will be important to extract accurate information.

2 Theoretical Aspects

2.1 DIS and Current Fragmentation

For inclusive inelastic scattering , individual events are characterized by the variables ν and Q^2. The differential cross section is parametrized in terms of the structure functions W_1 and W_2 such as [4]

$$\frac{d^2\sigma}{dQ^2 d\nu} = \frac{4\pi\alpha^2 E_1}{Q^4 EM}[W_2(Q^2,\nu)\cos^2\frac{\theta}{2} + 2W_1(Q^2,\nu)\sin^2\frac{\theta}{2}],$$

where Q^2 is the negative four-momentum transfer squared,

$$Q^2 = -q^2 = 4EE_1\sin^2\frac{\theta}{2},$$

$$\nu = E - E_1,$$

E is the incidental electron energy on a target with mass M, and E_1 is the electron energy after the scattering at a laboratory angle θ,

$$E_1 = \frac{E - \frac{W^2-M^2}{2M}}{1 + \frac{2E}{M}\sin^2\frac{\theta}{2}}.$$

W is the invariant mass of the virtual photon and the target nucleon system,

$$W^2 = M^2 + 2M\nu - Q^2.$$

At higher Q^2 and ν, inelastic scattering leaves the target in a continuum state. Under these conditions scaling functions $F_1 = W_1(Q^2,\nu)$ and $F_2 = \frac{\nu}{M}W_2(Q^2,\nu)$ are nearly independent of Q^2 and are directly related to the parton densities within the nucleon. In this Bjorken scaling region the DIS cross section can be expressed as [5]

$$\frac{d^2\sigma}{dxdy} = \frac{8\pi\alpha^2 ME}{Q^4}\{F_2(x,Q^2)[1-y] + xy^2F_1(x,Q^2) - \frac{M}{2E}xyF_2(x,Q^2)\},$$

where the Lorentzian invariant quantity x is the Bjorken scaling variable

$$x = Q^2/(2pq) = Q^2/(2M\nu),$$

and

$$y = \nu/E.$$

According to scaling theory, the structure functions depend strongly on x, but only weakly on Q^2. This implies that the nucleon is composed of nearly free point-like partons and the structure functions are related to the momentum densities of the partons within the nucleon.

For semi-inclusive hadron production (only one hadron detected), the hadron fragmentation function is defined as [6]

$$D^h(x, Q^2, z, p_T^2) = \frac{1}{\sigma(Q^2, x)} \frac{d^2\sigma^h}{dz dp_T^2}$$

where

$$z = \frac{E_h}{\nu}$$

is the fraction of the virtual photon energy absorbed by the hadron, P_T is the transverse (to $\vec{q}$) momentum of the detected hadron.

Due to the different time scales of the hard $\gamma^* - q$ collision and the subsequent hadronization, the cross section for the entire process can be factorized into the product of the initial quark distribution and a fragmentation function. Consequently, the fragmentation function is independent of x, but scales with z. Factorization enables us to separate the non-perturbative physics in hadronization from the perturbative hard scattering in a way as [6]

$$D^h(x, z) = \sum_q \epsilon_q(x) D_q^h(z),$$

where ϵ_q is the probability for a quark of type q to be involved in fragmentation, and

$$\epsilon_q = e_q^2 q(x) / \sum_i e_i^2 q_i(x),$$

where $q(x)$ is the probability that the quark q with charge e_q has a momentum fraction in the range from x to $x + dx$. D_q^h is the fragmentation function describing the production of a hadron h from the quark q.

After summing over P_T^2, [7] one obtains

$$D^h(x,z) = \frac{1}{\sigma_{tot}}\frac{d\sigma^h}{dz} = \frac{1}{N_e}\frac{dN^h}{dz},$$

where N_e is the number of DIS events , and N^h is the number of detected hadrons of type h.

According to jet universality, lepton scattering from a parton in a nucleon N contains the same information as electron-positron annihilation into a hadron pair. However, unlike the annihilation reaction, lepton scattering on a fixed target offers a unique way to study the fragmentation of compound quark states such as a diquark. As the struck quark recoils, initiating a fragmentation event, the rest of the nucleon will move reciprocally, undergoing a spectator or target fragmentation. Target fragmentation can be separated from quark fragmentation by considering the Feynman scaling variable x_F, defined by

$$x_F = P_L^*/P_{Lmax}^*,$$

where P_L^* is the longitudinal momentum component of the hadron with respect to the virtual photon direction in the center mass system, the maximum value of which is chosen as

$$P_{Lmax}^* = W/2.$$

Fragmentation of the struck quark is formed in the region of positive x_F, while target remnant favors negative x_F.

Current fragmentation can be depicted in the Breit frame, where the virtual photon is completely space-like with four-momentum $(\vec{P}, E) = (0, 0, -2xP, 0)$. Here, P is the momentum of the nucleon and xP is the momentum of the leading struck quark. After the collision, the struck quark carries a four momentum $(0, 0, -xP, 0)$ along the virtual photon direction. Hence, $Q = 2xP$ or $P = Q/(2x)$. The picture in Breit frame is an approximation to the case when transverse momentum of the quark is negligible compared to its total momentum or, equivalently, $P >> P_T$. By placing the hadron arm in the direction of $\vec{q}$ we will select those hadrons with low P_T, thus optimizing the conditions for a study of current fragmentation.

2.2 Effects In Nuclear Medium

In the study of nuclear modification of fragmentation functions in hadronization, there are a variety of effects which need to be understood, the LPM and the Cronin effect are among the most important ones.

2.2.1 The LPM Effect

In QED, bremsstrahlung radiation is suppressed relative to Bethe-Heitler when the radiation formation time is long compared to the mean-free path; this is the LPM (Landau-Pomeranchuck-Migdal) effect [8] [9] and it has been experimentally tested by E146 at SLAC [10]. The QCD analog of the LPM effect is characterized by a destructive interference between the induced gluon radiation amplitudes associated with multiple gluon exchange when the mean-free path, Λ, is short comparing to the formation time, $\tau_f >> \Lambda$. The inelastic suppression leads to a smaller cross section between the parton and the nuclear medium. The details can be found in [11, 12, 13]. Unlike QED, one can not measure directly the energy loss of a fast parton in QCD. It can only be evaluated by observing the final hadron product at different kinematic settings and different size of the target nucleus. Wang and Wang [14] calculated the double scattering process including the twist-4 contribution and found a nuclear correction to the fragmentation function in DIS as $\alpha_s A^{2/3}/Q^2$.

Brodsky suggested a condition for the appearance of the LPM effect in a discussion on Drell Yan process such as [15]

$$E_q > \mu^2 L_A,$$

where E_q is the quark energy in the laboratory frame, L_A is the size of the target nucleus, and μ is the mass difference between the incident quark and the quark-gluon pair. Wang and Wang [14] gave a formula for the gluon formation length as

$$\tau_f = 2Ez(1-z)/\ell_T^2,$$

where ℓ_T is the transverse momentum of the leading hadron. Kopeliovich

suggested a formation length for the DIS experiment at JLab as [16]

$$\tau_f = 2\nu/(Q^2 + P_T^2 + m_\pi^2).$$

Despite the difference in the representations of the formation length, both formulas have in common that the LPM effect favors high energy and small transverse momentum. Since the LPM effect can be treated as a twist-4 contribution, a moderate Q^2, such as that possible with JLAB beam energies, is adequate. The LPM effect is very important in the energy loss calculations for a parton traversing dense QCD matter as is the case at RHIC.

2.2.2 The Cronin Effect

It was found in pA reactions at high energies that the cross section for high-P_T single particle emission increases with A^α, α=1.1-1.4 and varies with particle type [17, 18]. This is the so called Cronin effect which leads to a broadening of P_T spectra, and the effect steeply rises with energy. The Cronin ratio for target nucleus A and B (A>B) is defined by [19]

$$R(P_T) = \frac{Bd\sigma_{pA}/d^2p_T}{Ad\sigma_{pB}/d^2p_T}.$$

In absence of nuclear effects, R is expected to be 1. The data showed an enhancement of the P_T spectra at P_T >1.0. The effect is understood as a multiple interactions of the parton in the nuclear matter [20, 21, 22]. P_T broadening has also been observed in eA [23] and Drell Yan process [24]. Hadron spectra at large P_T will help to determine the average parton energy loss in the medium generated in heavy ion collision [25].

2.3 Quark-gluon liquid

One of the challenging discoveries of 2005 was the so-called Quark-Gluon Liquid (QGL) [1,2,3], which was identified as one of the most important discoveries of the year. Since we presented the proposal in 2004, data from RHIC [2] have shown a jet quenching effect in central gold-gold collisions when P_T is

greater than 3 GeV, while the suppression is absent in d-Au scattering. The evolution of the hadronization process is shown schematically in Fig. 1. In the limit of infinitely high temperature the effective temperature-dependent coupling constant becomes small (asymptotic freedom). Consequently, the quark-gluon "plasma" should behave like an ideal gas and its properties be calculable using perturbative methods. However, it was proposed by the RHIC collaboration that instead of reflecting the existence of a hot, dense gaseous state, their data on relativistic heavy-ion collisions reflected the existence of a liquid state. The RHIC data are consistent with strong elliptical flow, strong jet quenching, small viscosity, and rapid thermalization corresponding to large parton cross sections. All of these indicate that the nuclear matter is behaving like an ideal fluid! This constitutes an exciting observation, which must be understood if we are to ever understand the mechanism by which hadronic matter emerged after the Big Bang. Fig. 2 shows a typical set of the RHIC data, in which gold-gold collisions at 200 GeV are compared to deuteron-gold collisions [3]. From the data, the jet quenching effect is striking as P_T exceeds 3 GeV.

The QGL is formed at high temperature and high matter density so the ensuing hadronization occurs in a very complicated environment. In order to understand the underlying physics, we first have to understand the basic processes and effects at low temperature, i.e., in cold matter. One of the best tools for studying these effects is deep inelastic lepton scattering from different nuclei. One important variable in heavy-ion collisions is P_T, the transverse momentum, which corresponds to the energy transfer ν of electron scattering. As we see in Fig. 2, jet quenching starts when P_T approaches 3 or 4 GeV/c. The current JLAB beam energy of $\approx$11 GeV is well matched to observation of the onset of jet quenching.

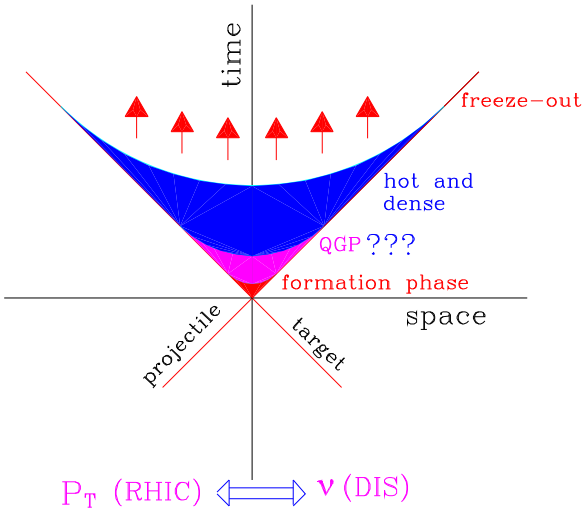

Figure 1: Skematic view of the evolution of hadronization after relativistic heavy ion collision.

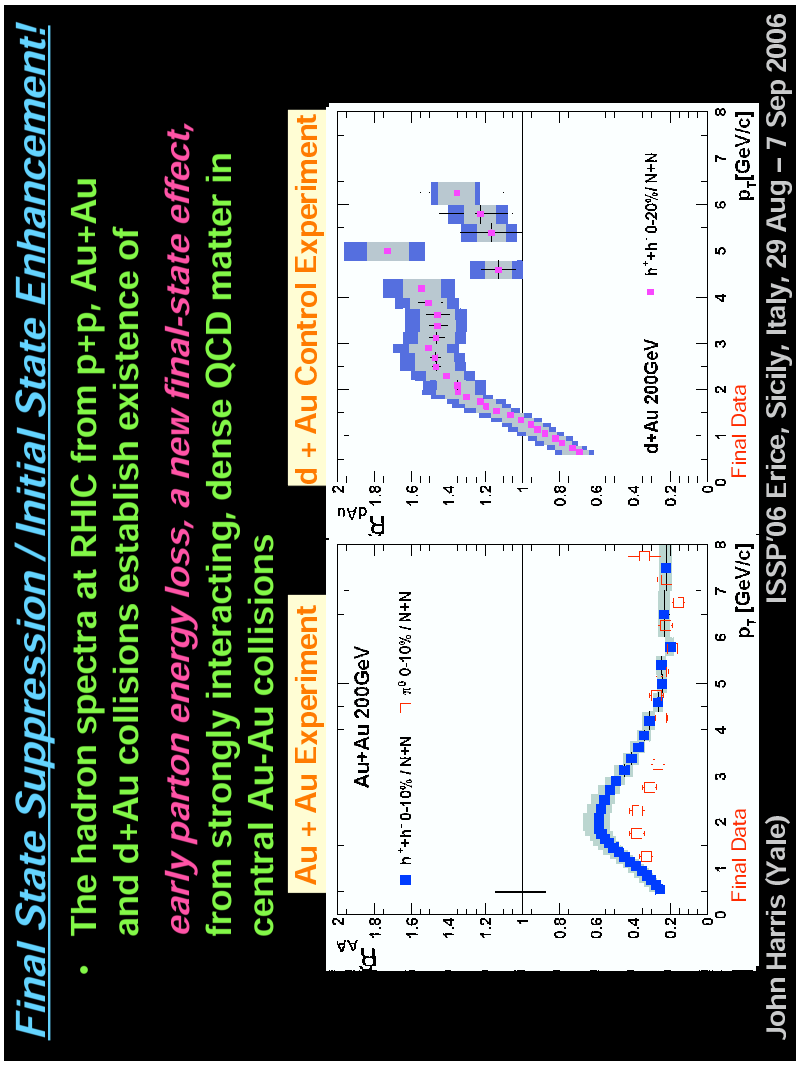

Figure 2: A typical set of the RHIC data from gold-gold collisions at 200 GeV is compared to that of deuteron-gold collisions [3].

2.4 Theoretical Work

One of the major outstanding problems in DIS is the theoretical description of the hadronization process. Even when the reaction occurs at high momentum transfer where PQCD (perturbative QCD) can be applied, the hadronization process is still dominated by non-PQCD contributions. Hence, phenomenological modeling is unavoidable. The most recent models are the Wang model [26] and Kopeliovich model [27]. In Wang model, modified quark fragmentation functions in DIS and the QCD evolution equations were derived in a framework of multiple parton scattering. The calculation from Kopeliovich [27] was compared with the HERMES data and found that the main source of nuclear suppression of the hadron production rate is attenuation of colorless pre-hadrons in the medium. On the other hand, the string models Lepto [28] [29] and the Venus model [30] [31] can be used as an experimental guidance. In these string models, a fast-moving quark forms a transversely confined color-flux tube. Hadrons are generated by a quark-antiquark pair in the color field. These models can predict the multiplicity, energy spectrum, and flavor distribution in the process of hadronization. The confinement caused by the color field explains the limited transverse momentum of the hadrons. In addition to these models, there was also the Feynman-Field (FF) model [32] [33] which emphasized the description of inclusive data. A fragmentation function was introduced to specify the probability that one of the leading quarks forms a hadron with a certain fraction of its momentum. It is successful in explaining the cross section but fails to describe correlation phenomena.

2.4.1 The Wang Model

The Wang model [26] is based on the fact that the partons generated in DIS will interact as they traverse the nuclear medium. The modified quark fragmentation functions are softened by induced radiation. It is assumed that the modification depends quadratically on the nuclear size. The predicted shape of the $z-$ and $\nu-$dependence agrees well with the experimental data.

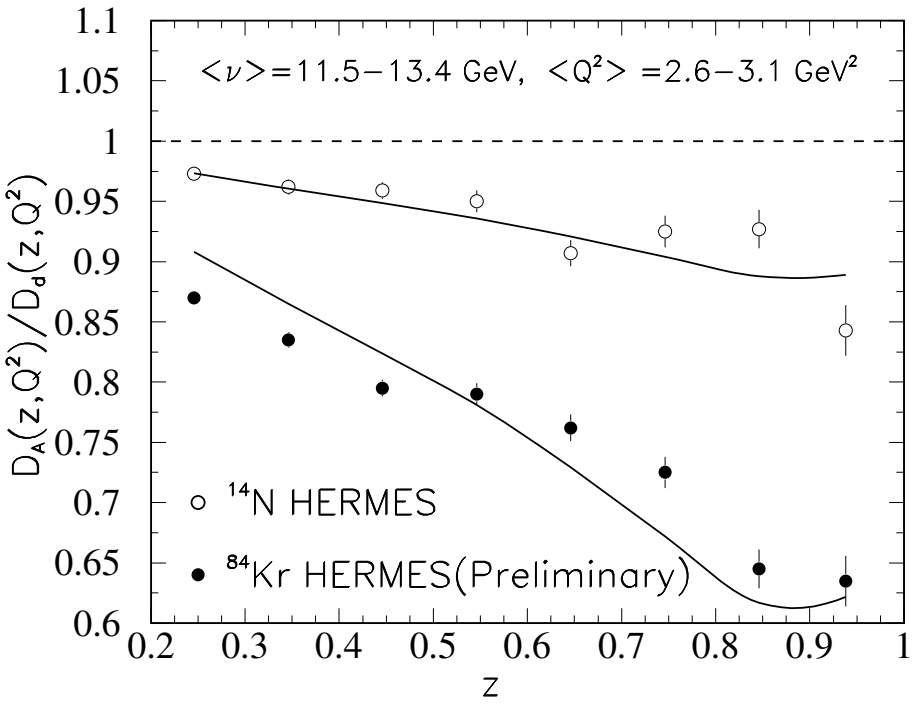

Figure 3: Calculated nuclear modification of fragmentation function by Wang in comparison with the HERMES data [34] of charged hadron.

A remarkable feature of the prediction is the quadratic $A^{2/3}$ nuclear size dependence, as shown in Fig. 3 [35]. The model supposes that the nuclear attenuation in this energy (27.5 GeV) region is mainly caused by induced gluon radiation and multiple parton scattering,

2.4.2 The Kopeliovich Model

In this model [27], a leading quark originated from DIS loses energy for hadronization which is treated perturbatively via gluon bremsstrahlung. In the case of in-medium hadronization the quark radiates more gluons due to multiple soft interaction with the medium. This correction is usually much smaller than the vacuum energy loss. Energy loss (both vacuum and induced) stops when color neutralization occurs, i.e. the leading quark picks up an antiquark and produces a pre-hadron, which is a colorless $\bar{q}q$ dipole with no stationary wave function. The corresponding time interval is called *the production time*, or production length. Energy conservation enforces the production time to vanish at the kinematic limit of production of hadrons with maximal possible energy ($z_h \to 1$).

The pre-hadron attenuates on its way out of the nucleus with an absorptive cross section which is controlled by the varying dipole size. Color transparency is an important ingredient of this dynamics. Eventually, on a longer time scale, called *formation time* (or length) the dipole develops the hadronic wave function. The model employs a quantum-mechanical description of this process within the light-cone Green function approach. Contrary to the production length vanishing at $z_h \to 1$, the formation length reaches a maximal value in this limit.

All these effects important for nuclear modification of the hadron production rate can be evaluated. Then the model is able to predict in a parameter free way the nuclear effects in DIS as function of energy, z_h, Q^2 and p_T. The predictions appear to be in agreement with HERMES data.

Searching for observables which are able to disentangle different models, Kopeliovich et al concluded that the energy loss scenario should have problems explaining the already available data for flavor and Q^2 dependence of

nuclear suppression. Their model is insensitive to the hadronic size, but the difference in fragmentation function at $z_h \rightarrow 1$ leads to more suppression for kaons than for pions. This is at variance with HERMES data. Also the comparison of data on different reactions at different hard scales led to a conclusion that p_T broadening and energy loss rise with Q^2. Such an expectation also contradicts HERMES data. They conclude that it would be very informative to have data on the variation of the p_T-distribution with z_h, which is a direct way to measure the production length.

2.4.3 The String Models

The Venus model [30][31] is a code to compute fragmentation of a string in a medium of hadrons; final state interactions (FSI) are included. The code is based on the dual parton model, in which an energetic lepton delivers a considerable amount of momentum to a quark in the nucleon via a virtual photon. The collision results in a quark-diquark string. Since the string is formed inside the nucleus, its space-time evolution will be different than if it were in the vacuum. The whole string or the later string fragments may interact with the spectator nucleons. The Lepto code [28] [29] is also a relativistic string model for fragmentation. The treatment of several jets is relativistic and it incorporates gluon radiation. Nuclear effects are not included.

2.4.4 The Macroscopic Model

The Bialas model is developed in a macroscopic way [36] which predicts the hadron attenuation without involving the details of the internal physics. The calculation is based on 'self-absorption' of the struck quark and the hadron formed from the quark. It folds the quark and hadron probabilities and the cross sections with the density distribution of the target nucleus, thereby including nuclear effects. In describing the DIS of a lepton at a point (b, z) inside the nucleus, the z-axis is the direction of the momentum transfer and b is the transverse dimension. If the characteristic time of the fragmentation is denoted by τ, the probability that the intermediate state at the point (b, z')

$(z' \geq z)$ is a quark is given by

$$P_q(z' - z) = exp[(z - z')/\tau],$$

and the probability that it is a hadronic fragment is given by

$$P_h(z' - z) = 1 - P_q(z' - z).$$

Combining the two expressions, one has the probability that neither the quark nor its fast fragment are absorbed by a single nucleon in the nucleus,

$$S_A(b, z) = 1 - \sigma_q \int_z^\infty dz' \rho_A(b, z') P_q(z' - z) - \sigma_h \int_z^\infty dz' \rho_A(b, z') P_h(z' - z),$$

where σ_q and σ_h are the cross sections for the absorption of the quark or hadron, ρ_A is the nuclear density. The Bialas model treats pions and nucleons equally.

3 Previous Data and Physics Motivation

3.1 Experimental Data

Nuclear effects on hadronization were first studied using DIS by Osborne *et. al.* at SLAC [37]. The electron beam energy was 20.5 GeV, the targets were hydrogen, deuterium, Be, C, Cu and Tn, Q^2 ranged from 0.35 to 5.0 $(\mathrm{GeV/c})^2$, while W^2 was between 7 and 31 $(\mathrm{GeV})^2$, P_T was less than 0.9 GeV/c, and x_F was positive. The data showed that there was an attenuation of forward going hadrons and that the attenuation increased with the atomic number A of the target nucleus. However, there was no visible broadening of the higher P_T component for different regions of z and for both positive and negative charged hadrons. A magnet dipole was used to separate particles by charge but no further particle identification was performed. Despite limited statistics (10k events per target) the results were quite interesting, since they revealed nuclear effects in the process of hadronization. This is the first experiment which demonstrated that the hadronic evolution can be studied by semi-inclusive DIS with nuclear targets.

Similar experiments subsequently were performed at CERN (EMC) [1] using muon beams with energies up to 175 GeV and targets such as C, Cu and Sn. It was found that at such energies, the struck quark travels a large distance and hadronizes outside the nuclear medium. Thus nuclear effects are weak due to the smaller cross section between the leading quark and the medium. Combining the experimental results from SLAC and CERN, it can be surmised that nuclear effects are more important when ν is small. Thus, they are more likely to be seen in lower energy experiments. Like the EMC data, the E665 results from FNAL obtained with a 490 GeV muon beam (TMC) [2] are far outside the energy region where nuclear effects can be significantly influential.

Most recently, the HERMES collaboration examined nuclear effects in the scattering of 27.5 GeV positrons from deuterium and nitrogen[34]. The data covered a range of ν from 7 to 23 GeV. Besides an attenuation of the hadron spectra, the data also showed different attenuations of positive and negative hadrons. Unlike in the SLAC data, a nuclear enhancement at high P_T is

observed in data from HERMES [23]. A sizable increase can be seen near P_T=0.6 GeV/c; the attenuation ratio reaches unity near P_T= 1 GeV/c for nitrogen and krypton as shown in Fig. 4. The broadening is stronger for heavier target nuclei. Recent results from HERMES [38] show similar broadening for all hadronic species as functions of z, ν, and Q^2. However, the statistics are such that no differences between species can be extracted and when plotted against each of the above kinematic quantities, the data have been summed over the other two quantities. While the data are suggestive, they are not sufficient to yield detailed answers.

The preliminary HERMES data at 12 GeV [39] covers ν values as low as 2.5 GeV, while the Q^2 is low with an average of about 0.9 (GeV/c)^2. Higher Q^2 data are required in order to ensure x-scaling at the low end of ν values.

A comparison between the experimental conditions of the proposed experiment and those from other experiments at different laboratories is presented in Table 1.

data	beam	E_0 (GeV)	ν (GeV)	Q^2 (GeV/c)^2
SLAC	e^-	20.5	3-17	0.35-5
EMC	μ	175	>10	> 2
TMC	μ	490	>100	0.1-150
HERMES	e^+	27	7-23	$< 2.5 >$
HERMES	e^+	12	2.5-9	$< 0.9 >$
Hall B	e^-	5.7	3-5	1.5-5
Hall C	e^-	11	6	2.82, 4.26, 5.99

Table 1: Comparison of the kinematics of the world data, the Hall B measurement, and the proposed Hall C experiment.

Following the HERMES data by several years, the CLAS EG2 (E02-104) experimental results opened a new vista in the field with its high statistics

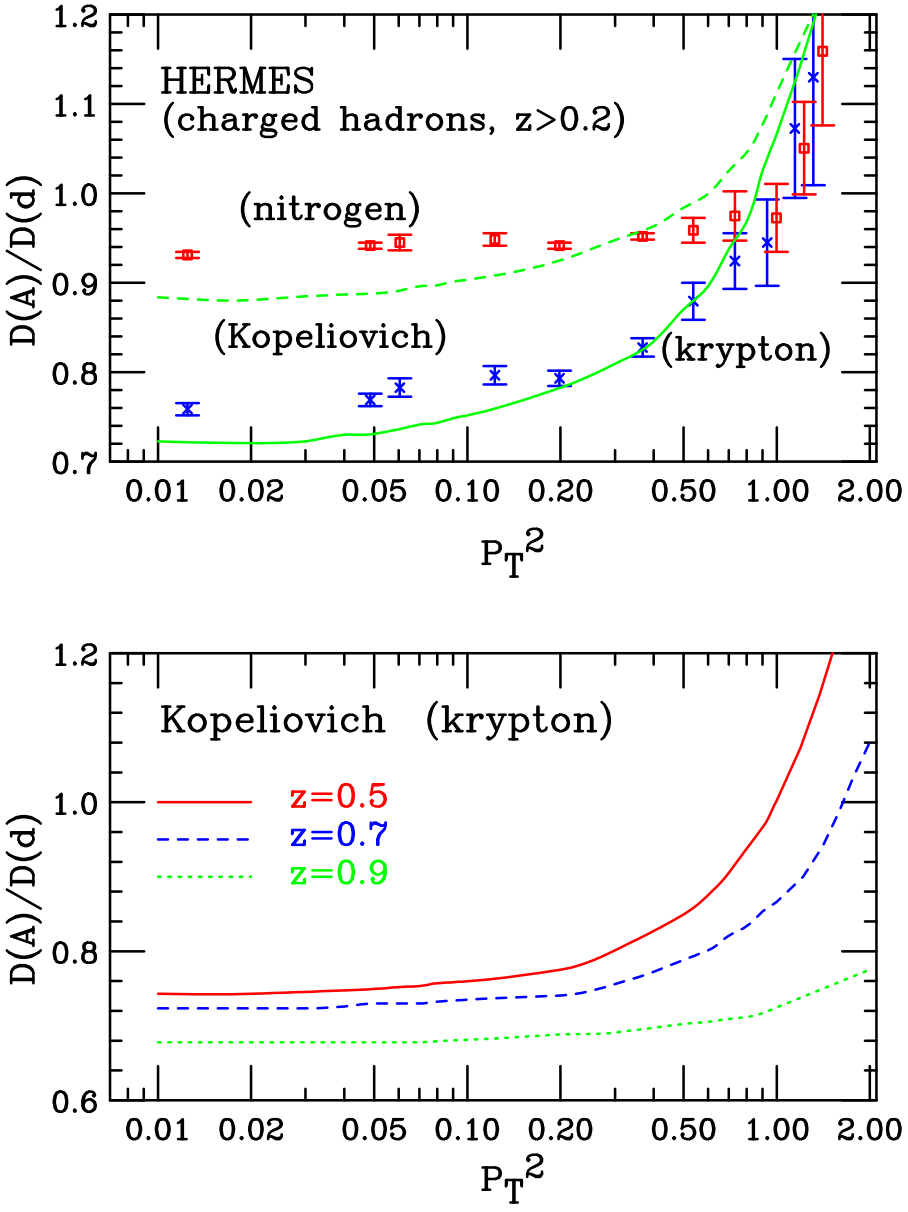

Figure 4: P_T dependence of nuclear attenuation. The top frame shows SLAC data (Cu plus Sn) [37] for negatively charged hadrons with $0.4 < z < 1.0$. The bottom frame shows HERMES data for charged hadrons [23]. Here, the upper band is for nitrogen and the lower band is for krypton.

and heavier targets. The EG2 data were taken in 2003 with 5 GeV electron beam and a luminosity of $10^{34}/cm^2/sec$. Both the multiplicity ratio and the transverse momentum broadening for carbon, iron, and lead were measured relative to deuterium. The multiplicity ratio is defined by

$$R(\nu, z, p_T, Q^2) = \frac{\frac{dN^h(A)}{N_e(A)dz}}{\frac{dN^h(D)}{N_e(D)dz}},$$

where p_T is the transverse momentum of the hadron and $z = E_h/\nu$ is the fraction of energy carried by the hadron. Fig. 5 [4] shows $< \Delta p_T^2 >$ vs the cube root of the atomic number of the target, $A^{1/3}$, and $< \Delta p_T^2 > = < p_T^2 >_A - < p_T^2 >_D$. Currently, the preliminary data involve the π^+ only, and the analysis for the other particles is under way. As shown in the Fig. 5, these data are obtained in a Q^2 range from 1 to 2 $(GeV/c)^2$, ν in a range of 2 to 3 GeV, and z from 0.5 to 0.6. The plot shows the transverse momentum broadening to be consistent with a linear dependence on the radius of the target nucleus. These beautiful measurements confirm that the quark energy loss has a quadratic dependence on the quark path length in the nuclear matter, a signature of the LPM effect in QCD. A recent analysis of the HERMES data [40] shows that the hadronic production rates cannot be described by a combination of the VENUS Model and a simple geometric model for absorption. The source of the discrepancy was traced to anomalously large differences between results for nitrogen and neon, differences which are under investigation.

Fig. 6 shows the Q^2 dependence of the multiplicity ratio of π^+ for ν in a range of 2 to 3 GeV and z between 0.5 and 0.6. In general, it is a very slowly varying function in the range of kinematics accessible in that experiment. The Q^2 dependence over a wider kinematic range is an important factor in the study of possible effects contributing to the hadronization process.

These preliminary data indicate that the final results from the CLAS EG2 experiment will be very helpful to our understanding of quark propagation in nuclear matter. They will shed light on two subjects, the hadronization process of the leading quark and the energy loss of the quark inside the nucleus.

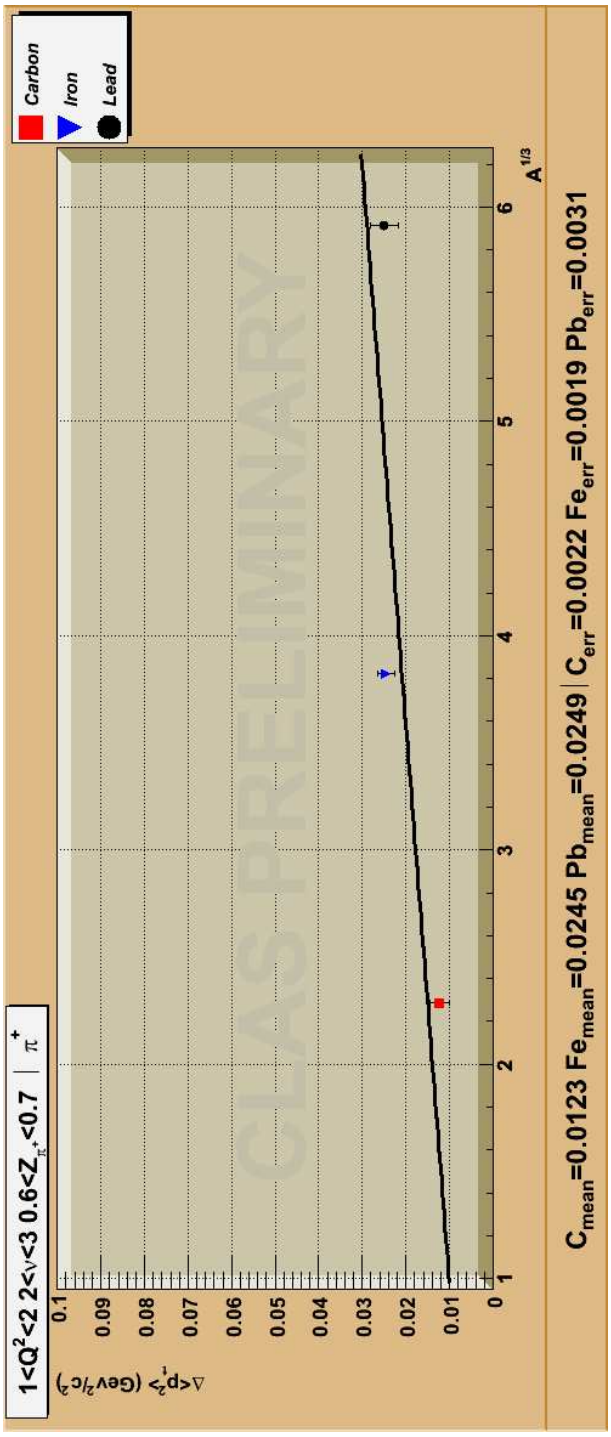

Figure 5: Preliminary CLAS data of ΔP_T^2 vs $A^{1/3}$ for π^+ on carbon, iron, and lead [5].

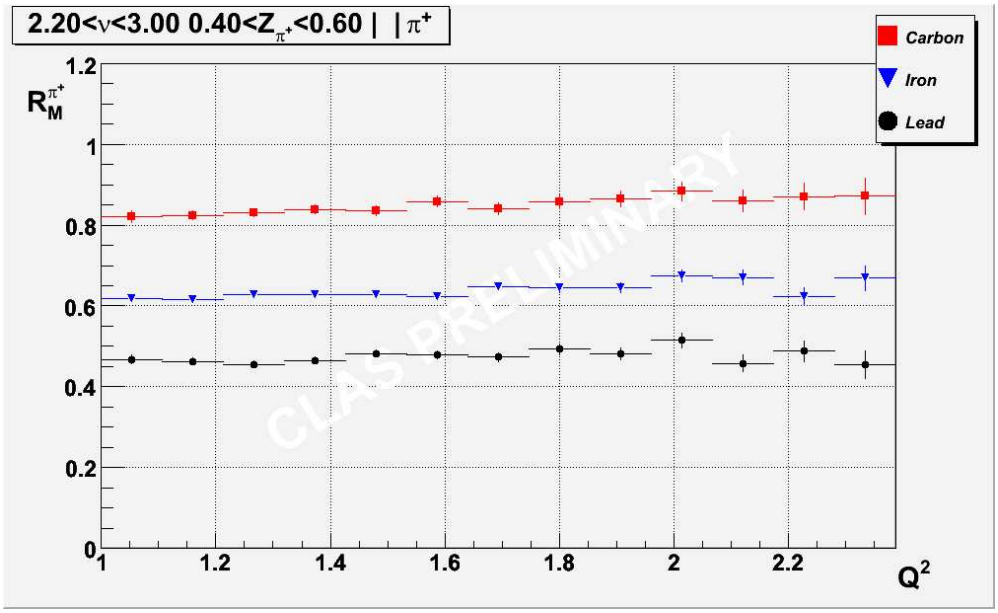

Figure 6: Preliminary CLAS data of the attenuation ratio as a function of Q^2 for π^+ on carbon, iron and lead [5].

Due to the QCD confinement and the very small space-time interval involved, quark propagation can only be studied indirectly by observing the hadron attenuation in nuclei of different sizes. Data from the proposed experiment, at higher Q^2 and higher ν will help in clarifying whether the hadrons can be formed inside or outside the heaviest available nuclei as well as provide insight into the mechanisms involved. The high luminosity, heavier target nuclei, and relatively modest beam energies will enable the new data to make significant and unique contributions to this exciting physics.

3.2 Motivation

The difficulty in the study of space-time evolution lies not only in the complicated process, but also in the limitation of the final hadronic observables. Hence, a carefully designed delicate experiment will be of great significance. In semi-inclusive DIS measurements, there are many variables and a variety of effects tangled together. A single effect or parameter could be influenced by several different variables and, vice versa, one variable could be sensitive to a couple of different effects. Apparently, any one-dimension spectrum with all the other dimensions integrated will not be sufficient to single out a specific effect or to fix a certain parameter. Unfortunately, for some large acceptance detectors, the kinematic coverage is often rather broad, from very low Q^2 to high, from small z to large. In this regard, small acceptance detectors serve as an indispensable device for focusing on a small kinematic region and for keeping all other dimensions at fixed values. The data will provide more rigorous constraints to models of this and related processes.

3.2.1 Formation Length

In DIS, a quark absorbs an energetic virtual photon and recoils along its direction. After a short distance it will materialize into a hadron or hadronic jet. Both the quark and the hadron(s) will interact with the nuclear medium during this interval. The interaction cross section for a hadron is typically about 20 mb, while the cross section for the quark is much smaller. In reference [34], a few different parameterizations for hadron formation length are listed:

$$\tau_h = z\nu,$$

$$\tau_h = (1-z)\nu,$$

and

$$\tau_h = (1-\ln(z))z\nu.$$

Clearly, these various forms generate different dependencies on z. Data from the proposed experiment will be used to evaluate the z-dependence of the formation length.

3.2.2 Testing Factorization

We will focus on higher Q^2 where the quark degrees of freedom dominate the coherent processes. As we view DIS from a frame with high momentum, the life time of a free quark is dilated as $\gamma\tau$, while the size of the nucleon is shortened as $1/\gamma$, hence, a free quark is more likely to be probed. At high Q^2, the influence of the nucleon degrees of freedom will be smaller. By comparing the data at two different different values of Q^2's but the same value of ν, one will be able to examine the validity of factorization.

3.2.3 Is the Hadron Formed Inside the Nucleus?

In the interpretation of the 27.5 GeV data, see Fig. 3, the HERMES collaboration suggested that the hadron attenuation is mainly caused by hadrons which are formed inside the nucleus [34]. However, according to Wang's calculation [14], the nuclear attenuation is mainly caused by induced gluon radiation and multiple parton scattering in the relevant energy region. Obviously, a solution for solving the puzzle is to push the energy scale ν down to lower values and to bring up the size of the target nucleus. This is another goal for the proposed experiment. Data will be taken at ν= 4 GeV and Q^2 reasonably high and the target nucleus will be extended to tungsten which is much bigger than the krypton that was used in the HERMES measurement. The powerful particle identification capability of the HRS serves as a key part of this effort. It is believed that different hadronic species have different cross sections especially below 10 GeV [19, 41]. If hadronization happens inside the nuclear medium, pions are expected to have a larger attenuation than kaons.

3.2.4 Is P_T Broadened?

The SLAC data [37] and the HERMES data [23][40] (Fig. 4) show different behaviors of the P_T spectra. The P_T broadening is a major issue in the heavy ion data interpretation. It is important to have a dedicated experiment to measure the P_T dependence in different kinematic regions and over a wide

range of nuclei. The experiment proposed here will take data in three separate P_T regions, from the lowest possible to a moderate 0.8 GeV/c. The results will determine whether the P_T spectra are broadened, as indicated by the HERMES result, or distributed more uniformly, as suggested by the SLAC measurement. Unlike both the SLAC and HERMES data, the proposed experiment can be sorted in to smaller bins for each dimension on each single hadron species and on each single target. Hence, the P_T dependence can be studied more precisely and more distinctly. In addition, the choice of heavier target nuclei (tungsten) will magnify the effect as compared to the krypton used in HERMES measurement.

3.2.5 Searching for the LPM Effect

As discussed in the previous chapter, the LPM effect will be likely to occur at lower transverse momenta. By orienting the hadron arm HRSL along the recoil direction, we automatically, are looking at those hadrons with the smallest P_T. Hence we have the most favorable conditions under which to search for the LPM effect. If the LPM dominates, we would see a smaller attenuation and a correction to the fragmentation function which scales with $A^{2/3}$ [14]. However, some other effect could possibly co-exist, such as P_T broadening (Cronin effect) and hadron interaction with the nuclear medium. To fully disentangle all these effects, we have to collect data at different kinematics by varying z, Q^2, A and m_h. In addition to the low P_T data, we also need a few measurements at moderate P_T. Since the multi-gluon exchange process can be described by the twist-4 expansion, measurement at a second Q^2 will help in testing the $1/Q^2$ [14] dependence. The data from light and heavy targets will make the observation of the LPM effect clearer via a comparison of the dependencies on $A^{1/3}$ and $A^{2/3}$ of the nuclear attenuation.

4 Experiment and Simulation

4.1 Detector Description

The HMS and SHMS spectrometers in Hall C will be used for this experiment. The parameters of the two spectrometers are summarized in Table 2.

	HMS	SHMS
detecting	e^-	$\pi^{\pm}$, $K^{\pm}$, p
Range of P_0 [GeV/c]	0.4 to 7.3	2.5 to 11
Range of θ	10.5 to 90	5.5 to 25
acceptance_P [%]	$\pm$10	-15 to +25
Resolution_p [%]	0.1 to 0.15	<0.2
solid angle [msr]	8.1	4 (LSA tune), 2msr (SSA tune)
$\delta\theta_H$ [mrad]	0.8	2 to 4
$\delta\theta_V$ [mrad]	1.0	1.0 to 2.0
e/h Discrimination	$> 1000:1$ at 98% efficiency	1000:1 at 98% efficiency
π/K Discrimination	100:1 at 95% efficiency	100:1 at 95% efficiency

Table 2: Comparison of HMS and SHMS parameters.

The SHMS is chosen for the hadron detection for two reasons: it has a higher maximum momentum which permits detection of the hadrons with larger z and it takes less time to change the central momentum. We will detect both positively charged (π^+, K^+ and proton) and negatively charged particles (π^- and K^-) in the SHMS. Separation of the various hadronic species will be required. The momentum resolution attainable with the SHMS is adequate.

The HMS will be used to detect electrons. The only specific requirement on the HMS is that it provide good identification of electrons. Its resolution is more than adequate to define the virtual photon with the necessary precision.

4.2 Kinematic Selection

Fig. 7 shows the phase space accessible with a 11 GeV electron beam. The two parallel solid lines (magenta) show the $Q^2 - \nu$ relationship for W=2 GeV and W=3 GeV. The two dashed lines (blue) show the relationship for x=0.2 and x=0.6. The lower bound of the DIS region is normally set at $Q^2 > 1$ (GeV/c)^2 and $W > 2$ GeV to meet the requirement of $x-$scaling. For the present experiment, we also require that $x > 0.2$ in order to suppress possible events from VMD or sea quark contributions. For an inclusive measurement, the available phase space is indicated by the hatched (yellow and green) area.

We propose to run the experiment at a ν value of 6.0 GeV. This will limit the scattered electron energy E_1 to 5.0 GeV. Hence, the three-momentum of the virtual photon q_3 is always greater than E_1. Equivalently, the angle of the recoil will always be smaller than that of the electron arm. Consequently, the minimum SHMS angle of 5.5° will place a lower limit on Q^2 as shown in Fig. 7 by the short curve (cyan). Two kinematic settings are planned for the electron arm corresponding to Q^2 = 2.82, 4.26 and 5.99 (GeV/c)^2. For the electron arm setting at Q^2=4.26 (GeV/c)^2, there will be four different angles for the hadron arm. For the other electron arm setting(Q^2=2.82 and 5.99) , there is one angle planned for the hadron arm Including each change on the hadron arm, we will need a total of 6 SHMS-HMS configurations, as listed in Table 3.

The purpose of setting 1 is to explore the z-dependence of the attenuation at low P_T. Setting 2 is aimed to detect negatively charged hadrons. For settings 3 and 4, the hadron arm detector will be off the momentum transfer direction and measurements of the P_T-dependence will be made. From a LEPTO prediction, settings 1, 3 and 4 together will cover a range of P_T from 0 to 0.8 GeV/c, which is deemed to be sufficient to search for P_T broadening.

Setting 5 and 6 at a higher Q^2 will be useful in testing the validity of factorization.

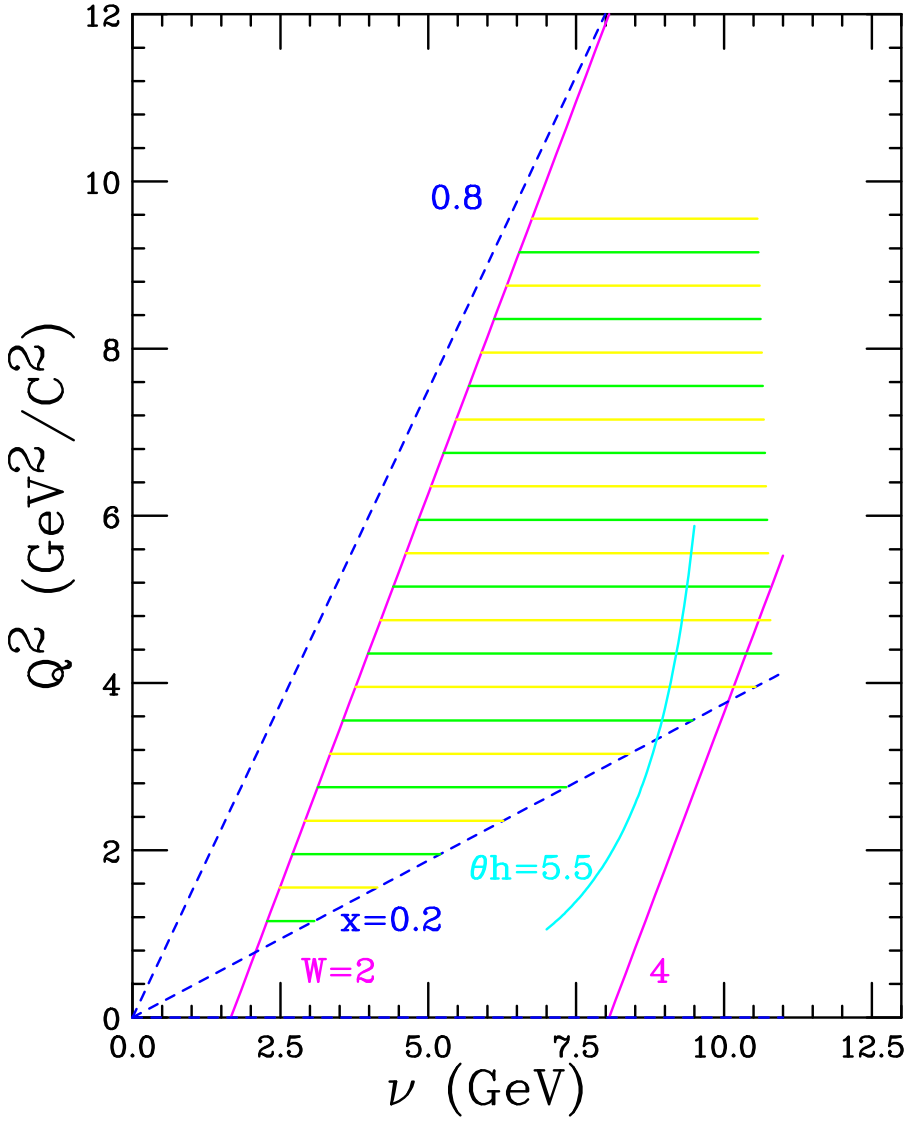

Figure 7: Phase space accessible with an incident electron energy of 11 GeV. The curves are described in the tex.

Kin	θ_e (deg.)	ν (GeV)	Q^2 (GeV/c)^2	θ_R (deg.)	θ_h (deg.)	B_h	N_P
1	16	6	4.26	12.61	11	+	4
2	16	6	4.26	12.61	11	−	4
3	16	6	4.26	12.61	18	+	4
4	16	6	4.26	12.61	23	+	4
5	13	6	2.82	10.00	10.0	+	3
6	19	6	5.99	14.39	14.39	+	3

Table 3: Kinematic parameters of the experiment. θ_e is the electron scattering angle, θ_R is the recoil angle (direction of $\vec{q}$), and θ_h is the angle of hadron arm detector. B_h is the polarity of the magnet and N_P is the number of momentum settings.

4.3 Target

Deuterium, carbon, copper and tungsten will be used as the target nuclei for this experiment. The characteristic parameters and the thickness are listed in Table 4. N_D is the equivalent number of deuterons per square centimeters. A liquid hydrogen target will also be mounted for calibration purposes.

4.4 Monte Carlo simulations

For the purpose of estimating kinematic distributions and event rates, the LEPTO program was used. The simulation was performed in two steps. First, for each setting and target different reaction products were generated. Second, the events were read back by an analyzer which produced histograms for each hadron species within the constraints of the angular and momentum acceptances of Hall C 12GeV.

The lower bound of the SIDIS region is normally set at $Q^2 > 1(GeV/c)^2$ and $W > 2GeV$ to meet the requirement of x-scaling. $x_F > 0$ is used to select

target	Z	A	$X_\circ$ (cm)	density (g/cm^3)	thick (cm)	N_D ($10^{23}/cm^2$)	radius (fm)
LH2	1	1	865	0.071	15	6.4	0.81
LD2	1	2	757	0.162	15	7.3	1.4
Carbon	6	12	18.8	2.265	0.75	5.1	2.6
Copper	29	64	1.43	8.96	0.072	1.93	4.49
Tungsten	74	184	0.35	19.3	0.02	1.15	6.38

Table 4: Target parameters. $X_\circ$ is radiation length, N_D is the equivalent number of deuterons per unit area.

those hadrons from current fragmentation. The momentum for hadrons is required to be higher than $1GeV$ and the $W' > 1.5GeV$

Fig. 8 to Fig. 11 show some observable distributions generated from the LEPTO code for π with the SIDIS cuts. Some observables for kaon are shown in Fig. 12.

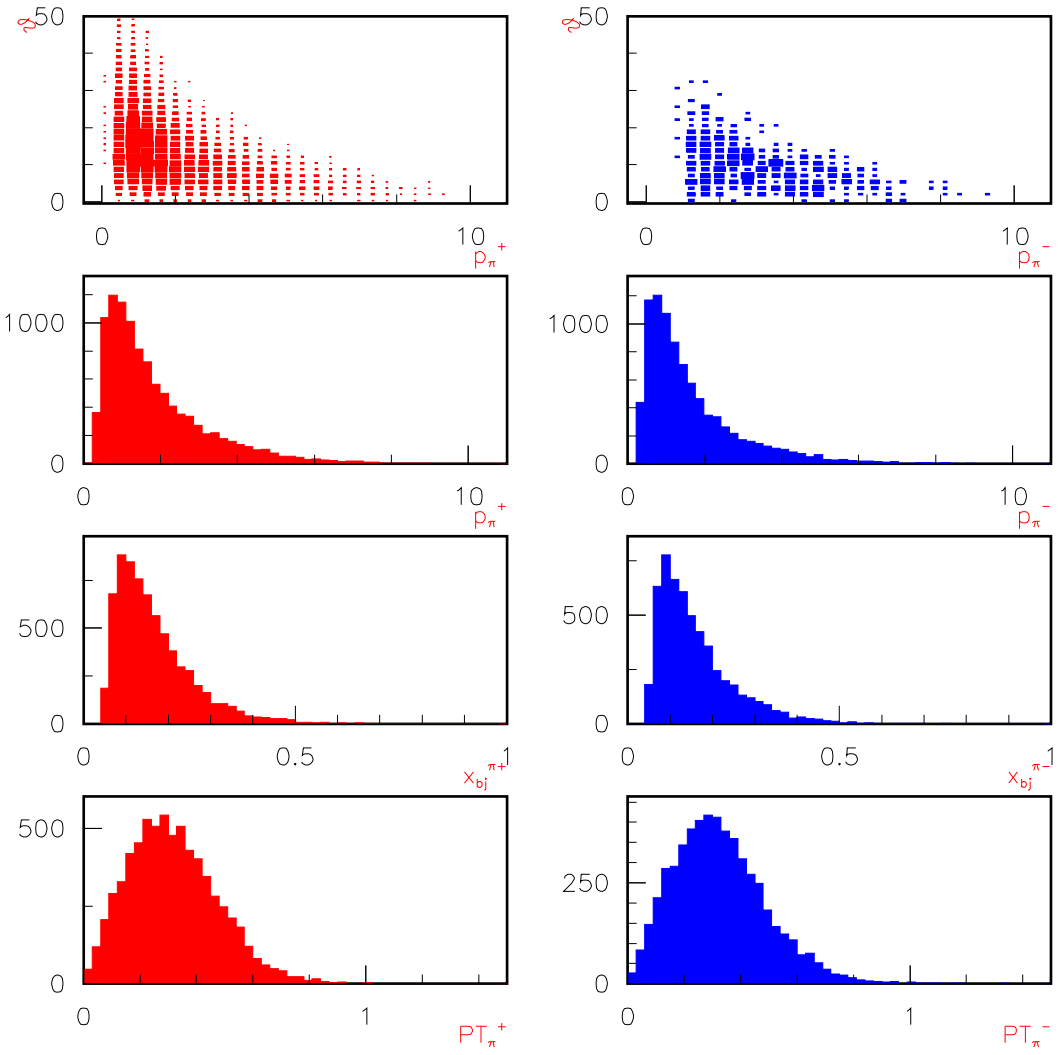

Figure 8: Hadron spectra (polar angle vs. momentum, momentum, x, and PT) for π^+(left) and π^-(right) from the LEPTO code assuming $\theta_e = 16°$, ν =6 GeV, a 11 GeV electron beam, and a deuteron target.

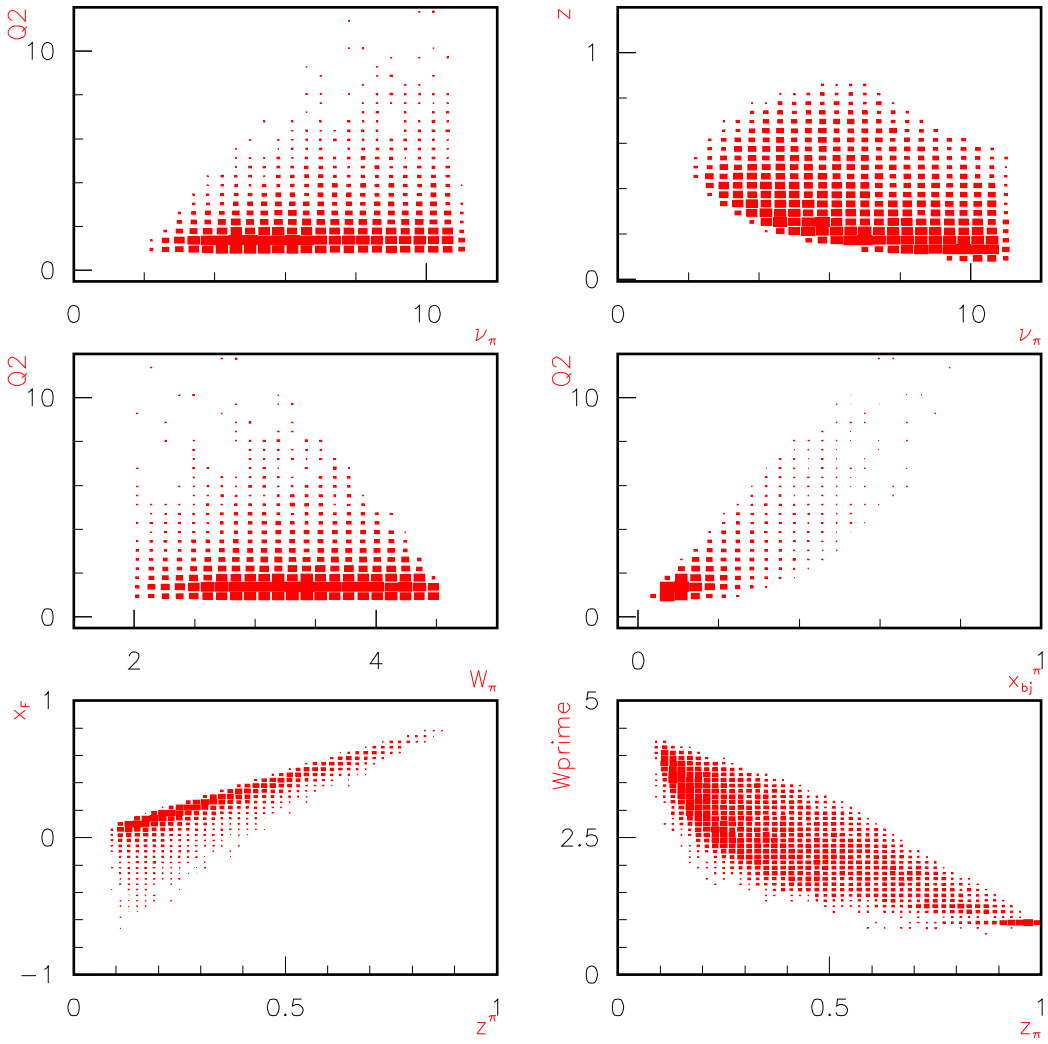

Figure 9: Hadron spectra (Q^2 and z vs. ν, Q^2 vs. W and x_{bj}, x and W' vs. z, where W' is the invariant mass of the hadronic system without the detected pion) for π from the LEPTO code assuming $\theta_e = 16°$, ν =6 GeV, a 11 GeV electron beam, and a deuteron target.

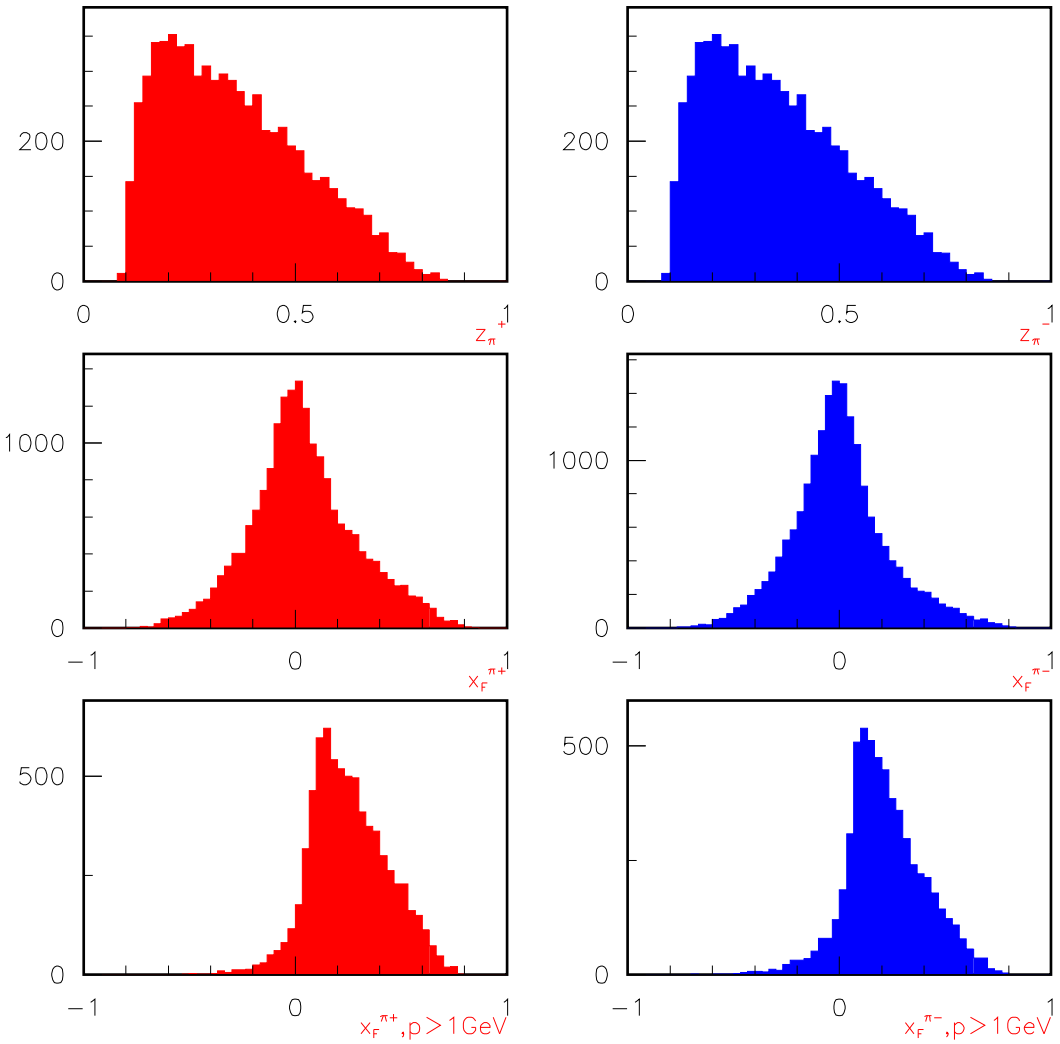

Figure 10: Hadron spectra (z, x_F, and x_F while p_π >1GeV) for π^+(left) and π^-(right) from the LEPTO code assuming $\theta_e = 16°$, ν =6 GeV, a 11 GeV electron beam, and a deuteron target.

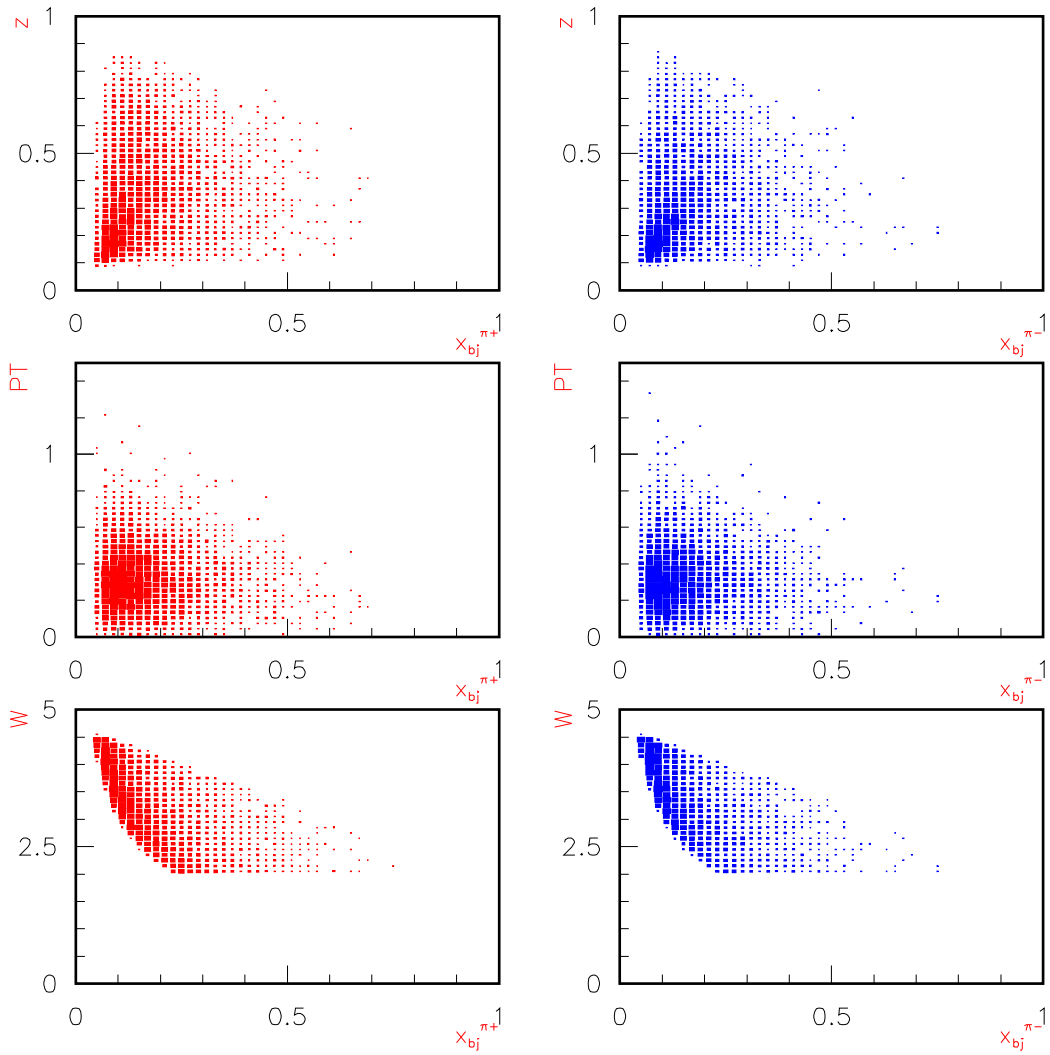

Figure 11: Hadron spectra (z, PT and W vs. x_{bj}) for π from the LEPTO code assuming $\theta_e = 16°$, ν =6 GeV, a 11 GeV electron beam, and a deuteron target.

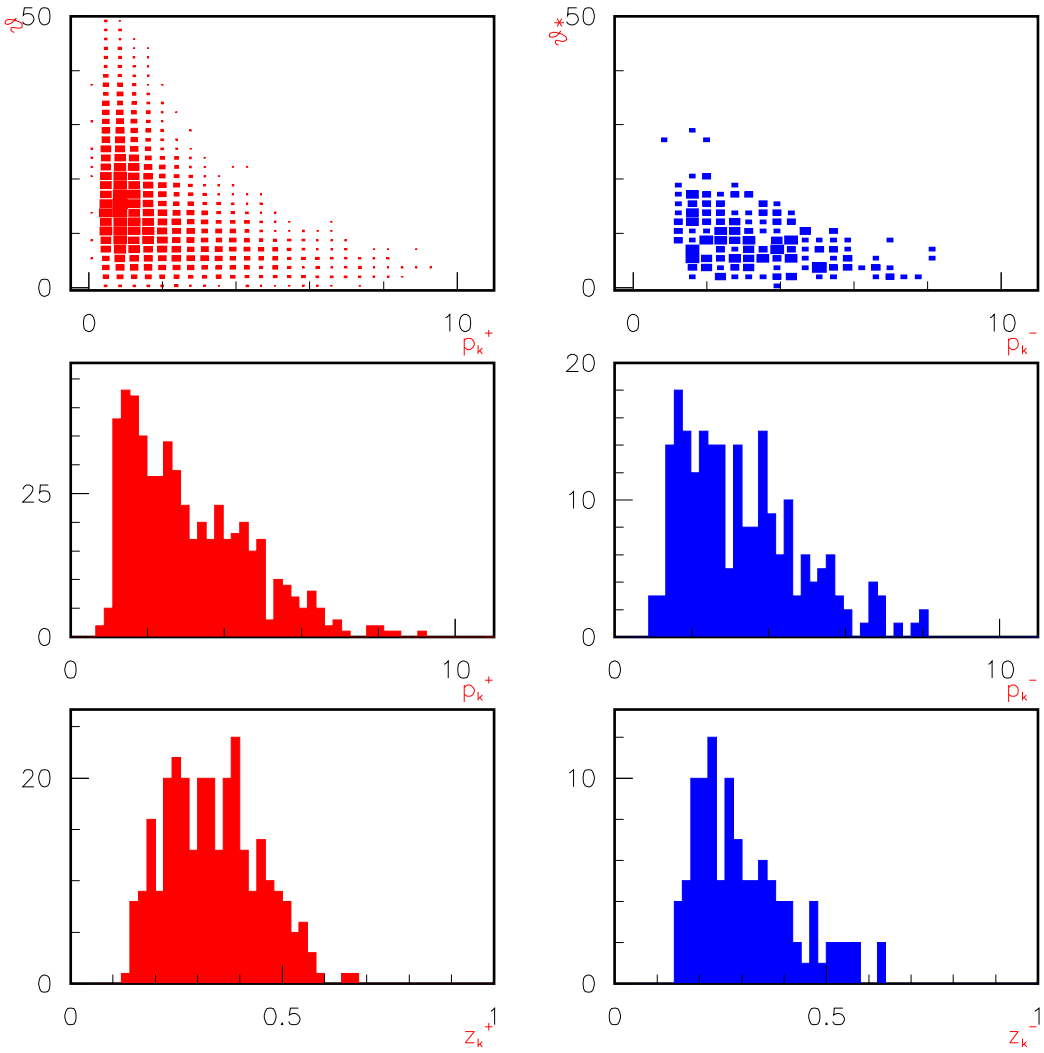

Figure 12: Hadron spectra (polar angle vs. momentum, momentum and z) for K^+(left) and K^-(right) from the LEPTO code assuming $\theta_e = 16°$, ν =6 GeV, a 11 GeV electron beam, and a deuteron target.

4.5 Cross Section and Rate Estimation

The estimation of the coincidence cross sections has the following inputs:

- The inclusive p(e, e') cross sections.
- Parameterizations of the fragmentation functions D_π^+ and D_π^-.
- A model of the transverse momentum distributions of pion and kaon as fragmentation products.

The inclusive deep inelastic (e, e') cross section can be expressed in the quark model as:

$$\frac{d^2\sigma}{d\Omega dE'} = \frac{\alpha^2(1+(1-y)^2)}{sxy^2}\frac{E'}{M_N\nu}\sum e_q^2 f_1^q(x)$$

where $s = 2EM_N + M_N^2$. The unpolarized quark distribution functions $f_1^q(x)$ and $f_1^{\bar{q}}(x)$ are taken from the CTEQ global fits. The semi-inclusive $(e, e'h)$ cross section relates to the quark fragmentation function $D_q^h(z))$ and the total inclusive cross section σ_{tot} through:

$$\frac{1}{\sigma_{tot}}\frac{d\sigma(e,e'h)}{dz} = \frac{\Sigma e_q^2 f_1^q(x) D_q^h(z)}{\Sigma e_q^2 f_1^q(x)}$$

.

Existing data indicate that the fragmented products follow a Gaussian-line distribution in transverse momentum.

We took a solid angle of 8 msr and a momentum acceptance of 10% for the HMS to estimate the rate, which is based on a 100 μA beam current and a 15 cm liquid deuterium target, which combine to give a luminosity of 10^{39} 1/cm^2/sec. For the SHMS, the solid angle is set to 4 msr and the momentum acceptance is set to 20%. Compared the count rates from the LEPTO simulation, the rates estimation for different kinematics are briefed in Table 5.

Kin	θ_e (deg.)	ν (GeV)	Q^2 (GeV/c)^2	θ_R (deg.)	θ_h (deg.)	e^- (Hz)	π^- (Hz)	π^+ (Hz)
1	16	6	4.26	12.61	11	4.3k	3.1k	3.6k
2	16	6	4.26	12.61	18	4.3k	1.4k	1.7k
3	16	6	4.26	12.61	23	4.3k	0.1k	0.2k
4	13	6	2.82	10.00	10.0	6.5k	5.2k	5.6k
5	19	6	5.99	14.39	14.39	0.8k	0.05k	0.07k

Table 5: e^- and $\pi^\pm$ rate estimation for different kinematics proposed.

4.6 Beam Time Request

The beam time assignment for each kinematic sub-setting is listed in Table 6, 7 and 8. The total momentum coverage will lead to a selection of hadrons with z varying from 0.6 to 0.9, which is adequate to the purpose of the proposed experiment.

Table 9 is a summary of the time requested for data taking, where the time for auxiliary operations related to momentum changes (10 minutes), target changes (30 minutes), polarity changes (4 hours), and the relocation of HRSL (1 hour) is estimated at 2 hours for each move. The total time requested is 325 hours or about 13.5 days. In addition, we need 1.5 days for calibration and set up. Therefore, we are asking for 15 days in total.

P_c (GeV/c)	D (hour)	C (hour)	Cu (hour)	W (hour)
2.63	1	1	3	5
2.88	1	1	3	5
3.15	1	1	3	5
3.45	1	1	3	5
sum	4	4	12	20

Table 6: Beam time assignment for kinematic settings 1 and 2. P_c is the central momentum of SHMS.

P_c (GeV/c)	D (hour)	C (hour)	Cu (hour)	W (hour)
2.63	2	2	6	10
2.88	2	2	6	10
3.15	2	2	6	10
3.45	2	2	6	10
sum	8	8	24	40

Table 7: Beam time assignment for kinematic settings 3 and 4.

4.7 Projected Results

By analyzing the events obtained from the LEPTO code, we can fill various histograms for each independent parameter, such as z, P_T, and A for each well identified hadron species. These spectra can be used as a general guide for kinematic coverage and the precision of the projected data.

The predicted z spectra are plotted in Fig. 13 for π^+ and proton. The solid curves are calculations from the Bialas model [36], which treats all the hadrons as identical. According to the LEPTO code, the protons are

P_c (GeV/c)	D (hour)	C (hour)	Cu (hour)	W (hour)
2.88	2	2	6	8
3.15	2	2	6	8
3.45	2	2	6	8
sum	6	6	18	24

Table 8: Beam time assignment for kinematic setting 5.

Kin	data (hour)	Aux (hour)
1	40	4
2	40	8
3	80	9
4	80	5
5	54	4
total	294	30

Table 9: Overall beam time request for data acquisition.

suppressed more than the pions. The data will be used to compare with calculations [42] [43] based on the Wang model. This model predicts a strong drop for higher z values and for heavier target nuclei. The drop is probably due to the redistribution of the events and the shift of the events from higher to lower z's. The shape of the $z-$dependence will be useful in extracting the formation time.

Fig. 14 shows the ν-dependence of hadron attenuation and the Bialas calculation at $z = 0.65$; where curve a (Dashes, blue) is the calculation for A= 12; curve b (dotted, cyan) is the calculation for A= 64; and curve c (solid, green) is the calculation for A= 184. The HERMES data represented by '+' (blue) were chosen from $z > 0.5$ for charged pion and summed over the whole Q^2 and P_T range. The predicted data for the proposed experiment for π^+ at

$z = 0.65 \pm 0.5$ are shown with red diamonds (carbon), red circles (copper) and red boxes (tungsten) at $\nu = 4$ GeV. One can see the importance of pushing ν down to 4 GeV in that the attenuation is larger there.

Fig. 15 shows the P_T-dependence of the hadron attenuation for carbon, copper and tungsten and three z bins at $z = 0.65 \pm 0.5$, $z = 0.75 \pm 0.5$ and $z = 0.85 \pm 0.5$. Comparing the predicted P_T spectra to the SLAC and HERMES data (Fig. 4), the proposed data will not only have higher precision, but also smaller bins in all other dimensions and will be sorted for each specific hadron species explicitly. Since the broadening is stronger for heavier target nuclei and since tungsten nuclei are much bigger than krypton, the JLab measurement will be more sensitive to the multiple scattering effect. Therefore, the data will be sufficient to resolve the discrepancy on P_T broadening between the SLAC and the HERMES data.

Fig. 16 shows the A-dependence of π^+ attenuation at $z = 0.65 \pm 0.5$, $z = 0.75 \pm 0.5$ and $z = 0.85 \pm 0.5$. A good measurement of A-dependence is significant in examining whether the hadron is formed inside the nuclear medium. By comparing with Wang model, the A-dependence will also be able to show a coherent contribution related to the LPM effect.

The above histograms reflect only a part of the predicted data. Since there are three bins in z, eight bins in P_T, three target nuclei and five types of hadrons. There will be a lot more independent histograms of z, P_T, A, and hadron type. The large number of histograms will provide rich and unambiguous information which could turn out to be selectively sensitive to a certain effect or process. The results from the proposed experiment will provide stringent tests to a various theoretical models and will thus add important input to the analysis of RHIC data.

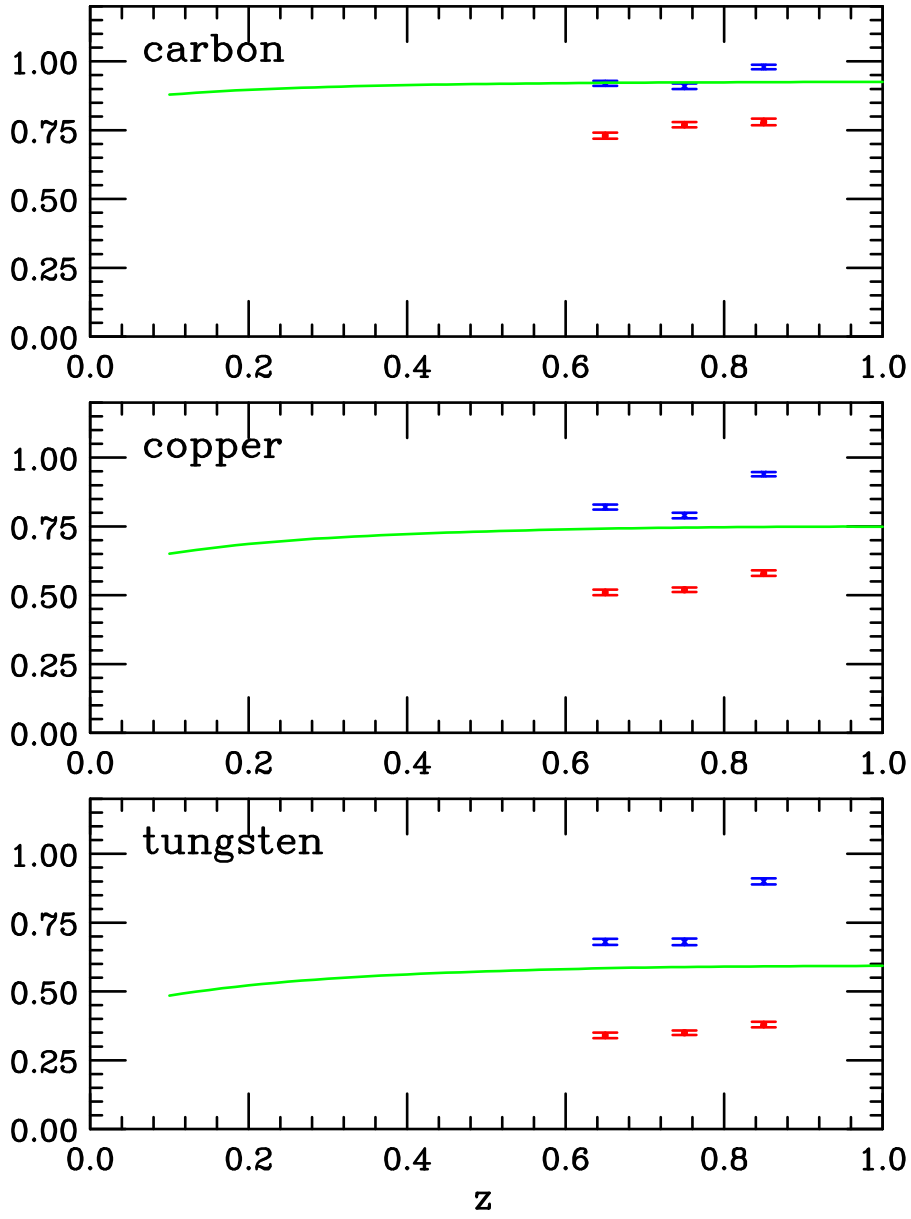

Figure 13: Attenuation of π^+ (blue x, larger) and proton (red o, smaller) in carbon (top), copper (central) and tungsten (bottom) as a function of z for $Q^2 = 2.82(GeV/c)^2$, $\nu = 6$ GeV and P_T= 0-0.25 GeV/c.

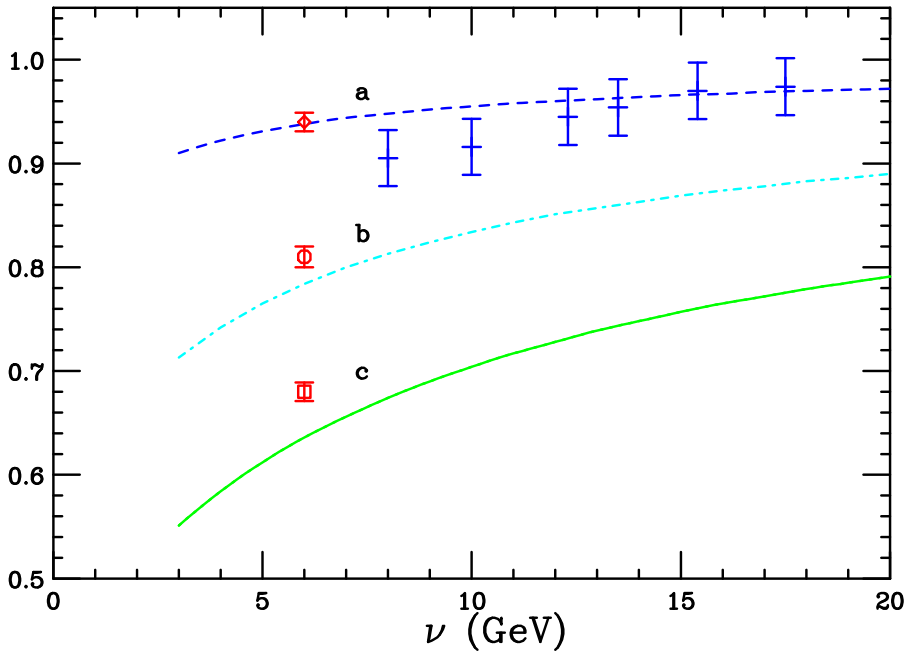

Figure 14: Attenuation of hadron as a function of ν, curve a (dashes, blue) for carbon, curve b (dash-dotted, cyan) for copper, curve c (solid, brown) for tungsten. The data point (red) at 6 GeV is projected for π^+ at $z = 0.65$. The Hermes data are taken at $z > 0.5$ for charged pions and summed over all the other kinematic variables.

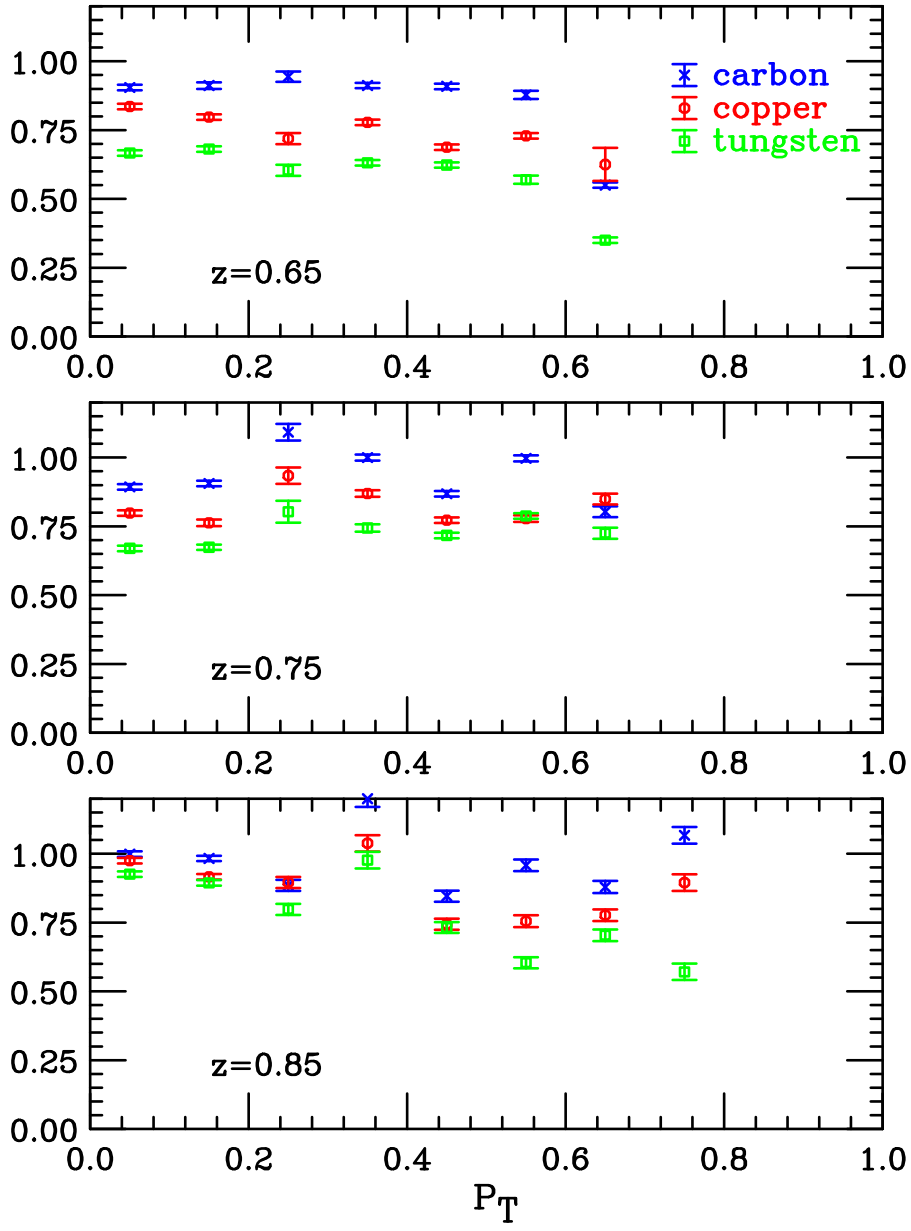

Figure 15: Attenuation of π^+ in carbon, copper and tungsten as a function of P_T for three different values of z. The data are simulated at $Q^2 = 2.82(GeV/c)^2$ and $\nu = 6GeV$. The uncertainty is statistics only.

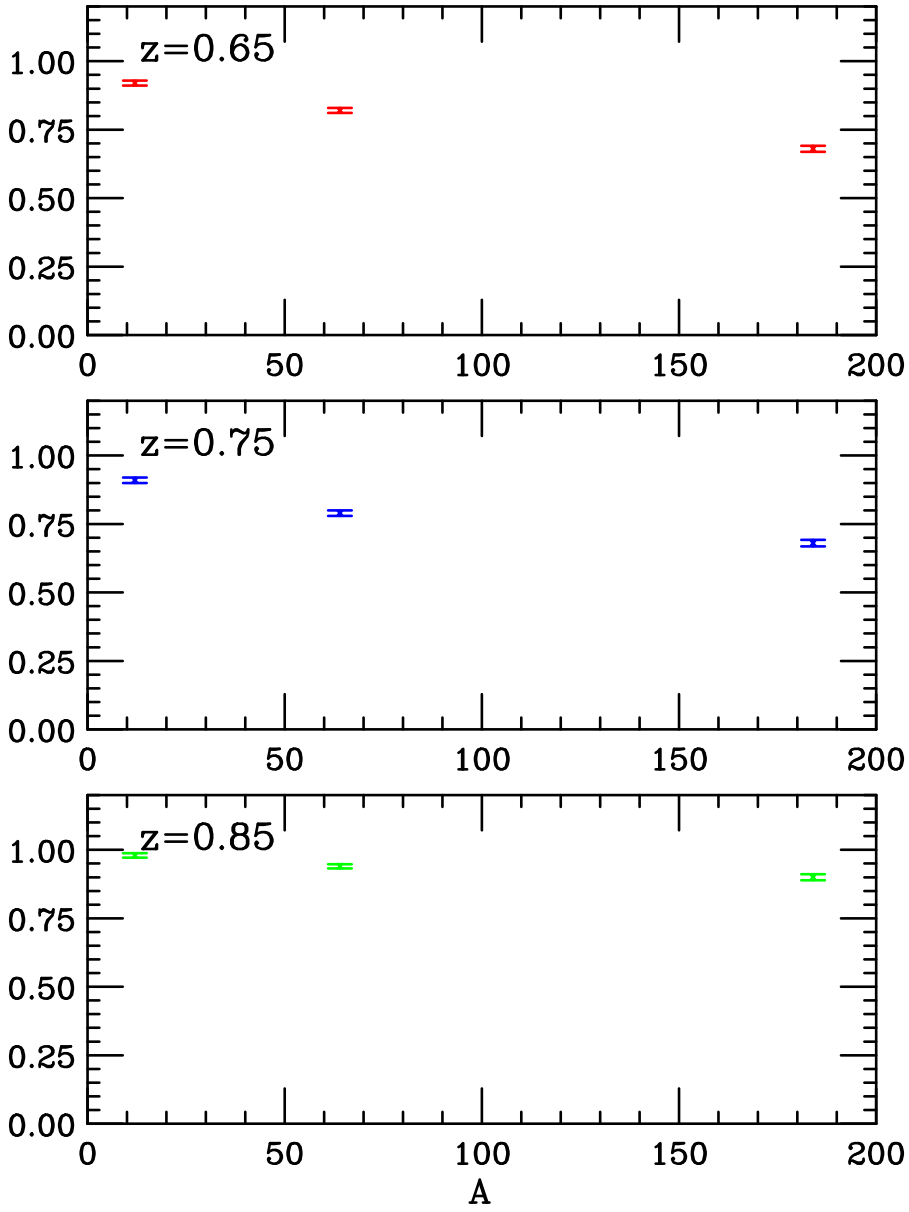

Figure 16: Attenuation of π^+ as a function of A for three different values of z. The data are simulated at $Q^2 = 2.82(GeV/c)^2$, $\nu = 6GeV$. The uncertainty is statistic only.

5 Summary

We propose to study current fragmentation by deep inelastic electron scattering with a 11 GeV electron beam on deuterium, carbon, copper and tungsten targets. The attenuation of hadrons will be extracted for each hadronic species. Dependence on Q^2, x, P_T, z, m_h and A will be explicitly obtained. The high statistics and high resolution results will shed light on the formation time in hadronization, quark re-scattering in the nuclear medium, as well as a possible observation of the LPM effect. The data with $\nu = 6$ GeV at $Q^2 = 2.82$, 4.26 and 5.99 $(GeV/c)^2$ will serve as an important input to the interpretation of RHIC data.

We request 15 days beam time, of which 1.5 days will be used for detector set up and calibration; 13.5 days will be devoted to data acquisition.

A Comparison to Other Experiments

The general physics issues to be addressed with the proposed experiment parallel those of an approved Hall-B proposal, E12-06-117 [44]. However, the high degree of kinematic selectivity made possible by the the high luminosity make the Hall-C experiment ($10^{39} cm^{-2} s^{-1}$) a necessary complement to the Hall-B experiment ($10^{35} cm^{-2} s^{-1}$). The studies proposed here will focus on the high Q^2 and high z regions where E12-06-117 will obtain limited data. In addition, we will be able to separate π and K mesons over the full momentum range whereas in E12-06-117 this separation will be possible for momenta up to 2-3 GeV/c, corresponding to a limit of about 0.5 for z for $\nu \approx 6\ GeV$.

Due to the small acceptance of HMS, data can be taken in very small bins of both Q^2 and ν. By locating HMS at specific angles, we can select the events at higher Q^2 without being overwhelmed by much more probable low Q^2 processes. The small cross section can be compensated by the high luminosity at Hall-C. With this feature, it will be possible to check the variation of the attenuation with Q^2 and x, to determine whether it is really as small as predicted. On the other hand, the current fragmentation study at low energy requires hadrons with large z; i.e., hadrons with momenta above 2 GeV/c. However, the hadron spectra peak at low momentum. The SHMS will be used to selectively isolate events involving energetic hadrons in the final state. Similarly, it will be possible to select data at larger, well defined values of P_T by changing the angular orientation of SHMS. This will be of fundamental importance to the study of QCD color confinement and quark re-interaction. The high resolution will enable us to optimize the kinematics to be sensitive to possible QCD effects which depend on Q^2 and ν.

Since hadrons of different types with large momentum are involved, we need to compare the differences in hadronization for pions, kaons and protons. Therefore, particle identification will play an important role. The HMS to be used for hadron detection is equipped with aerogel Cherenkov and RICH detectors (CsI-freon) which will offer excellent separation of kaon from pion over the full momentum range of our measurement. The pion and kaon separation is especially significant for large z where it will help in determining whether the hadron is formed inside the nucleus.

References

[1] J. Ashman *et al.*, Z Phys. **52**, 1 (1991).

[2] M. R. Adams *et al.*, Phys. Rev. D **50**, 1836 (1994).

[3] J. D. Bjorken, in Current Induced Reactions, Lecture Notes Physics 56, Ed. J.G. Korner et al., 1975.

[4] D. Perkins, Introduction to high energy physics, 1987, 3rd edition.

[5] P. property data booklet, Phys. Lett **B239**, 241 (1990).

[6] P. Renton and W. S. C. Williams, Ann. Rev. of Nucl. and Part Scin **31**, 193 (1981).

[7] T. Sloan, Physics Report **162**, 46 (1988).

[8] L. Landau and I. Pomeranchuk, Dikl. Akad. Nauk SSSR **92**, 92 (1953).

[9] A. Migdal, Phys. Rev. **103**, 1811 (1956).

[10] P. Anthony *et al.*, Phys. Rev. Lett. **75**, 1949 (1995).

[11] M. Gyulassy and X.-N. Wang, Nucl. Phys. B **420**, 583 (1994).

[12] X.-N. Wang *et al.*, Phys. Rev. D **51**, 3436 (1995).

[13] V. Baier and V. Katkov, Phys. Rev. D **57**, 3146 (1988).

[14] E. Wang and X. Wang, hep-ph/0202105, 2003.

[15] S. J. Brodsky, Color transparency and hadronzation in the nucleus, SLAC-PUB-4551, 1988.

[16] B. Kopeliovich, private communication, Aug, 2003.

[17] J. Cronin *et al.*, Phys. Rev. D **11**, 3105 (1975).

[18] D. Antreasyan *et al.*, Phys. Rev. D **19**, 764 (1979).

[19] A. Accardi, hep-ph/0212148, 2003.

[20] M. Johnson *et al.*, Phys. Rev. C **63**, 035203 (2001).

[21] B. Kopeliovich *et al.*, nucl-th/9607036, 1996.

[22] B. Kopeliovich *et al.*, hep-ph/0201010, 2002.

[23] V. Muccifore *et al.*, hep-ex/0106088, 2001.

[24] P. McGaughey, J. Moss, and J. Peng, Annl. Rev. of Nucl. and Part. Science **49**, 217 (1999).

[25] N. Xu, Nucl. Phys. A **610**, 175c (1996).

[26] X. Guo and X.-N. Wang, Phys. Rev. Lett **85**, 3591 (2000).

[27] B. Kopeliovich *et al.*, hep-ph/0311220, 2003.

[28] G. Ingelman, A. Edin, and J. Rathsman, code Lepto, http://www3.tsl.uu.se/thep/lepto., 1996.

[29] B. Ansderson *et al.*, Phys Rep **97**, 31 (1983).

[30] K. Werner and P. Koch, Z. Phys. C **47**, 215 (1990).

[31] K. Werner, Venus code, private communication.

[32] R. Field and R. P. Feynman, Nucl. Phys. B **136**, 1 (1978).

[33] R. Field and R. P. Feynman, Phys. Rev. D **15**, 2590 (1977).

[34] A. Airapetian *et al.*, Eur. Phys. J. C. **20**, 479 (2001).

[35] E. Wang and X.-N. Wang, hep-ph/0202105, 2002.

[36] A. Bialas, Phys. Lett **133B**, 241 (1983).

[37] L. S. Osborne *et al.*, Phys. Rev. Lett. **40**, 1624 (1978).

[38] Y. V. Haarlem *et al.*, hep-ph/0704.3712, 2007.

[39] H. Collaboration, http://www-hermes.desy.de/notes/pub.

[40] K. Fialkowski and R. Wit, hep-ph/0705.4354, 2007.

[41] P. Tables, Phys. Rev. D **54**, 192 (1996).

[42] X.-N. Wang, Wang model calculation, private communication.

[43] W. Brooks *et al.*, Jlab proposal E02-014, 2002, quark propagation through cold QCD matter.

[44] K. Hafidi *et al.*, Jlab proposal E12-06-117, 2006, quark Propagation and Hadron Formation.